Why Does Little Robustness Help? A Further Step Towards Understanding Adversarial Transferability

Yechao Zhang*[1,2,3,4], Shengshan Hu*[1,2,3,4], Leo Yu Zhang†, Junyu Shi*[1,2,3,4]
Minghui Li‡, Xiaogeng Liu*[1,2,3,4], Wei Wan*[1,2,3,4], and Hai Jin§[1,2,5]

* *School of Cyber Science and Engineering, Huazhong University of Science and Technology*
‡ *School of Software Engineering, Huazhong University of Science and Technology*
† *School of Information and Communication Technology, Griffith University*
§ *School of Computer Science and Technology, Huazhong University of Science and Technology*
[1]*National Engineering Research Center for Big Data Technology and System*
[2]*Services Computing Technology and System Lab* [3]*Hubei Key Laboratory of Distributed System Security*
[4]*Hubei Engineering Research Center on Big Data Security* [5]*Cluster and Grid Computing Lab*

{ycz,hushengshan,shijunyu220,minghuili,liuxiaogeng,weiwan_0303,hjin}@hust.edu.cn, leo.zhang@griffith.edu.au

***Abstract*—Adversarial examples for *deep neural networks* (DNNs) are transferable: examples that successfully fool one white-box surrogate model can also deceive other black-box models with different architectures. Although a bunch of empirical studies have provided guidance on generating highly transferable adversarial examples, many of these findings fail to be well explained and even lead to confusing or inconsistent advice for practical use.**

In this paper, we take a further step towards understanding adversarial transferability, with a particular focus on surrogate aspects. Starting from the intriguing "little robustness" phenomenon, where models adversarially trained with mildly perturbed adversarial samples can serve as better surrogates for transfer attacks, we attribute it to a trade-off between two dominant factors: model smoothness and gradient similarity. Our research focuses on their joint effects on transferability, rather than demonstrating the separate relationships alone. Through a combination of theoretical and empirical analyses, we hypothesize that the data distribution shift induced by off-manifold samples in adversarial training is the reason that impairs gradient similarity.

Building on these insights, we further explore the impacts of prevalent data augmentation and gradient regularization on transferability and analyze how the trade-off manifests in various training methods, thus building a comprehensive blueprint for the regulation mechanisms behind transferability. Finally, we provide a general route for constructing superior surrogates to boost transferability, which optimizes both model smoothness and gradient similarity simultaneously, *e.g.*, the combination of input gradient regularization and *sharpness-aware minimization* (*SAM*), validated by extensive experiments. In summary, we call for attention to the united impacts of these two factors for launching effective transfer attacks, rather than optimizing one while ignoring the other, and emphasize the crucial role of manipulating surrogate models.

1. Introduction

Adversarial transferability is an intriguing property of adversarial examples (AEs), where examples crafted against a surrogate DNN could fool other DNNs as well. Various techniques [8, 9, 18, 24, 35, 56, 63, 64] have been proposed for the generation process of AEs to increase transferability[1], such as integrating momentum to stabilize the update direction [8] or applying transformations at each iteration to create diverse input patterns [56]. At a high level, all these research endeavors to find transferable AEs under given surrogate models by proposing complex tricks to be incorporated into the generation pipeline one after another. However, this approach could result in non-trivial computational expenses and low scalability [38].

With a different perspective, another line of work starts to examine the role of surrogate models. One useful observation is that attacking an ensemble of surrogate models with different architectures can obtain a more general update direction for AEs [1, 28]. A recent study [17] also proposed fine-tuning a well-trained surrogate to obtain a set of intermediate models that can be used for an ensemble. However, it remains unclear which type of surrogate performs the best and should be included in the ensemble. Our work taps into this line and tries to manipulate surrogates to launch stronger transfer attacks.

Meanwhile, Demontis *et al*. [5] started to explain the transferability property and showed that model complexity and gradient alignment negatively and positively correlate with transferability, respectively. Lately, Yang *et al*. [58] established a transferability lower bound and theoretically connected transferability to two key factors: model smoothness and gradient similarity. Model smoothness captures the general invariance of the gradient *w.r.t.* input features

1. We refer to "adversarial transferability" as "transferability".

for a given model, while gradient similarity refers to the alignment of the gradient direction between surrogate and target models. However, there is still much to be understood and explored regarding these factors. For instance, it is unclear which factor plays a more important role in regulating transferability, how existing empirical findings for improving transferability affect these factors, and how to generally optimize them both simultaneously. Such a complex situation makes it challenging to completely understand the role of surrogates. Consequently, there is currently no consensus on how to construct better surrogates to achieve higher adversarial transferability. In support of this, a recent work [32], after performing a large-scale empirical study in real-world settings, concluded that surrogate-level factors that affect the transferability highly chaotically interact and there is no effective solution to obtain a good surrogate except through trial and error.

In light of this, we aim to deepen our understanding of adversarial transferability and provide concrete guidelines to construct better surrogates for boosting transfer attacks. Specifically, we offer the following contributions:

Gaining a deeper understanding of the "little robustness" phenomenon. We begin by exploring the intriguing "little robustness" phenomenon [44], where models produced by small-budget adversarial training (*AT*) serve as better surrogates than standard ones (see Fig. 2). Through tailored definitions of gradient similarity and model smoothness, we recognize this phenomenon comes along with an inherent trade-off effect between these two factors on transferability. Thus we attribute the "little robustness" appearance to the persistent improvement of model smoothness and deterioration of gradient similarity. Further, we identify the observed gradient dissimilarity in *AT* as the result of the data distribution shift caused by off-manifold samples.

Investigating the impact of data augmentation on transferability. Beyond *AT*, we explore more general distribution shift cases to confirm our hypothesis on data distribution shift impairing gradient similarity. Specifically, we exploit four popular data augmentation methods, Mixup (*MU*), Cutmix (*CM*), Cutout (*CO*), and Label smoothing (*LS*) to investigate how these different kinds of distribution shifts affect the gradient similarity. Extensive experiments reveal they unanimously impair gradient similarity in different levels, and the degradation generally aligns with the augmentation magnitude. Moreover, we find different augmentations affect smoothness differently. While *LS* benefits both datasets, other methods mostly downgrade smoothness in CIFAR-10 and show chaotic performance in ImageNette. Despite their different complex trade-off effects, they consistently yield worse transferability.

Investigating the impact of gradient regularization on transferability. As the concept of gradient similarity is inherently tangled up with unknown target models, it is difficult to directly optimize it in the real scenario. Therefore, we explore solutions that presumably feature better smoothness without explicitly changing the data distribution, *i.e.*, gradient regularization. Concretely, we explore the impact of four gradient regularizations on model smoothness: input gradient regularization (*IR*) and input Jacobian regularization (*JR*) in the input space, and explicit gradient regularization (*ER*) and sharpness-aware minimization (*SAM*) in the weight space. Our extensive experiments show that gradient regularizations universally improve model smoothness, with regularizations in the input space leading to faster and more stable improvement than regularizations in the weight space. However, while input space regularizations (*JR*, *IR*) produce better smoothness, they do not necessarily outperform weight space regularizations like *SAM* in terms of transferability. We also find this aligns with the fact that they weigh differently on gradient similarity, which plays another crucial role in the overall trade-off.

Proposing a general route for generating surrogates. Considering the practical black-box scenario, we propose a general route for the adversary to obtain surrogates with both superior smoothness and similarity. This involves first assessing the smoothness of different training mechanisms and comparing their similarities, then developing generally effective strategies by combining the best elements of each. Our experimental results show that input regularization and *SAM* excel at promoting smoothness and similarity, respectively, as well as other complementary properties. Thus, we propose *SAM&JR* and *SAM&IR* to obtain better surrogates. Extensive results show our methods significantly outperform existing solutions in boosting transferability. Moreover, we showcase that the design is a plug-and-play method that can be directly integrated with surrogate-independent methods to further improve transferability. The transfer attack results on three commercial *Machine-Learning-as-a-Service* (MLaaS) platforms also demonstrate the effectiveness of our method against real-world deployed DNNs.

In summary, we study the complex trade-off between model smoothness and gradient similarity (see Fig. 1) under various circumstances and identify a general alignment between the trade-off and transferability. We call for attention that, for effective surrogates, one should handle these two factors well. Throughout our study, we also discover a range of observations correlating existing conclusions and viewpoints in the field. Tab. 1 provides a glance at them and reports the relations.

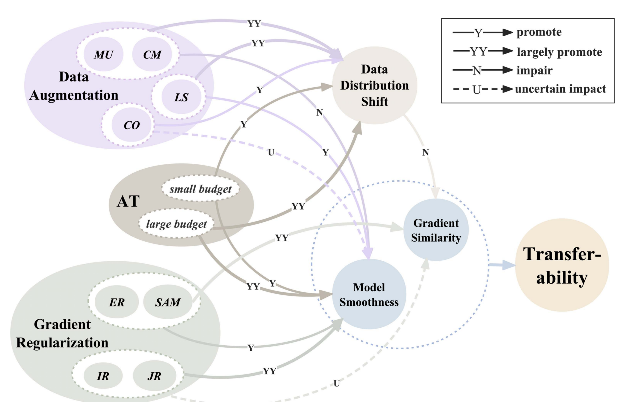

Figure 1: A complete overview of the relationship between factors regulating adversarial transferability in our study

TABLE 1: The overview of our interactions with literature in the field

Existing conclusions and viewpoints	Our observations and inferences	Relation
Stronger regularized (smoother) models provide better surrogates on average [5].	(1) *AT* with large budget yields smoother models that degrade transferability. In Sec. 2.1. (2) Stronger regularizations cannot always outperform less smooth solutions like *SAM*. In Sec. 4.3.	Partly conflicting
AT and data augmentation do not show strong correlations to transfer attacks in the "real-world" environment [32].	(1) *AT* with small budget benefits transfer attack while large budget hinders it. (2) Data augmentation generally impairs transfer attacks, especially for stronger augmentations. In Sec. 6, **Q6**.	Conflicting
Surrogate models with better generalization behavior could result in more transferable AEs [50].	Data augmentations that yield surrogates with the best generalization perform the worst in transfer attacks. In Sec. 6, **Q4**.	Conflicting
Attacking multiple surrogates from a sufficiently large geometry vicinity (LGV) benefits transferability [17].	Attacking multiple surrogates from arbitrary LGV of a single superior surrogate may degrade transferability. In Sec. 5.2.	Partly conflicting
Regularizing pressure transfers from the weight space to the input space. [7].	This transfer effect exists, yet is marginal and unstable. In Sec. 4.2.	Partly conflicting
The poor transferability of ViT is because existing attacks are not strong enough to fully exploit its potential [36].	The transferability of ViT may have been restrained by its default training paradigm. In Sec. 6, **Q5**	Parallel
Model complexity (the number of local optima in loss surface) correlates with transferability [5].	A smoother model is expected to have less and wider local optima in a finite space. In Sec. 6, **Q3**	Causal
AEs lie off the underlying manifold of clean data [15].	Adversarial training causes data distribution shift induced by off-manifold AEs, thus impairing gradient similarity.	Dependent
(1) Attacking an ensemble of surrogates in the distribution found by *Bayes* learning improves the transferability [25]. (2) *SAM* can be seen as a relaxation of Bayes [34].	*SAM* yields general input gradient alignment towards every training solution. Attacking *SAM* solution significantly improves transferability. In Sec. 6, **Q7**.	Matching

2. Explaining Little Robustness

Understanding adversarial transferability is still a challenging task, and many empirical observations in the literature are rather perplexing. As a typical case, *"little robustness"* indicates that a model adversarially trained with small perturbation budgets improves the transferability [44, 45]. It remains unclear why small-budget adversarially trained models can serve as better surrogates, whereas large-budget ones do not exhibit this benefit. In this section, we tailor the definitions of gradient similarity and model smoothness, two recently proposed concepts that are believed to be important for transferability [58], to analyze this phenomenon.

Notations. We denote the input space as $\mathcal{X} = \mathbb{R}^d$, and the output space as $\mathcal{Y} = \mathbb{R}^m$. We also consider a standard classification training dataset $\mathbf{S} = \{(x_1, y_1), \cdots, (x_n, y_n)\}$, where $x_i \in \mathcal{M} \subset \mathcal{X}$ and $y_i \in \mathcal{L} = \{(0,1)^m\} \subset \mathcal{Y}$ are *identically and independently distributed* (i.i.d.) drawn from the normal data distribution $\mathcal{D} \in \mathcal{P}_{\mathcal{X}\times\mathcal{Y}}$. $\mathcal{M}$ denotes the normal (image) feature manifold, $\mathcal{D}$ is supported on $(\mathcal{M}, \mathcal{L})$ and $\mathcal{P}_{\mathcal{X}\times\mathcal{Y}}$ is the set of distributions on $\mathcal{X} \times \mathcal{Y}$. We further denote the marginal distribution on $\mathcal{X}$ and $\mathcal{Y}$ as $\mathcal{P}_{\mathcal{X}}$ and $\mathcal{P}_{\mathcal{Y}}$, respectively. The classification model can be viewed as a mapping function $\mathcal{F} : \mathcal{X} \to \mathcal{L}$. Specifically, given any input $x \in \mathcal{X}$, $\mathcal{F}$ will find an optimal match $\mathcal{F}(x) = \arg\min_{y\in\mathcal{L}} \ell_{\mathcal{F}}(x, y)$ with the hard labels $\mathcal{L}$, where $\ell_{\mathcal{F}} : \mathcal{X} \times \mathcal{Y} \to \mathbb{R}_+$ can be decomposed to a training loss ℓ[2] and the network's logits output $f(\cdot)$: $\ell_{\mathcal{F}}(x, y) := \ell(f(x), y), (x, y) \in (\mathcal{X}, \mathcal{Y})$.

In this paper, we denote the surrogate model and target model as $\mathcal{F}$ and $\mathcal{G}$, respectively. Generally, both $\mathcal{F}$ and $\mathcal{G}$ can be trained within the data distribution $\mathcal{D}$ using $\mathbf{S}$, or a close yet different distribution $\mathcal{D}'$ obtained by a specific augmentation mechanism on $\mathbf{S}$. Throughout this paper, we use $\mathcal{D}'$ to denote a data distribution different from $\mathcal{D}$. Since this paper focuses on studying the transferability from the surrogate perspective, we assume $\mathcal{G}$ is also well-trained on $\mathcal{D}$ by default. We defer the analysis and results when $\mathcal{G}$ is trained on various $\mathcal{D}'$ to Sec. 6, **Q2**, where the results also support the conclusions drawn from the case of $\mathcal{D}$.

2. We use the cross-entropy loss by default in the paper.

2.1. Transferability Circuit of Adversarial Training

Adversarial training [30] (*AT*) uses adversarial examples generated on $\mathbf{S}$ as augmented data and minimizes the following adversarial loss:

$$L_{adv} = \frac{1}{\|\mathbf{S}\|} \sum_{i=1}^{\|\mathbf{S}\|} \max_{\|\delta\|_2 < \epsilon} \ell(f(x_i + \delta), y_i), \tag{1}$$

where $\delta \in \mathbb{R}^d$ denotes the adversarial perturbation and ϵ is the adversarial budget. As evidenced by our experiments in Fig. 2, the *attack success rates* (ASRs) rise with relatively small-budget adversarial trained models and start to decrease with the high-budget ones. This "transferability circuit" is particularly intriguing. We thus revisit the recently proposed transferability lower bound [58] and utilize it as a tool to analyze the underlying reason.

2.2. Lower Bound of Transferability

We first re-define model smoothness, gradient similarity, and the transferability between two models, based on which a lower bound of transferability can be obtained.

Definition 1 (Model smoothness). *Given a model $\mathcal{F}$ and a data distribution $\mathcal{D}$, the smoothness of $\mathcal{F}$ on $\mathcal{D}$ is defined as $\sigma_{\mathcal{F},\mathcal{D}} = \mathbb{E}_{(x,y)\sim\mathcal{D}}[\sigma(\nabla_x^2 \ell_{\mathcal{F}}(x, y))]$, where $\sigma(\cdot)$ denotes the*

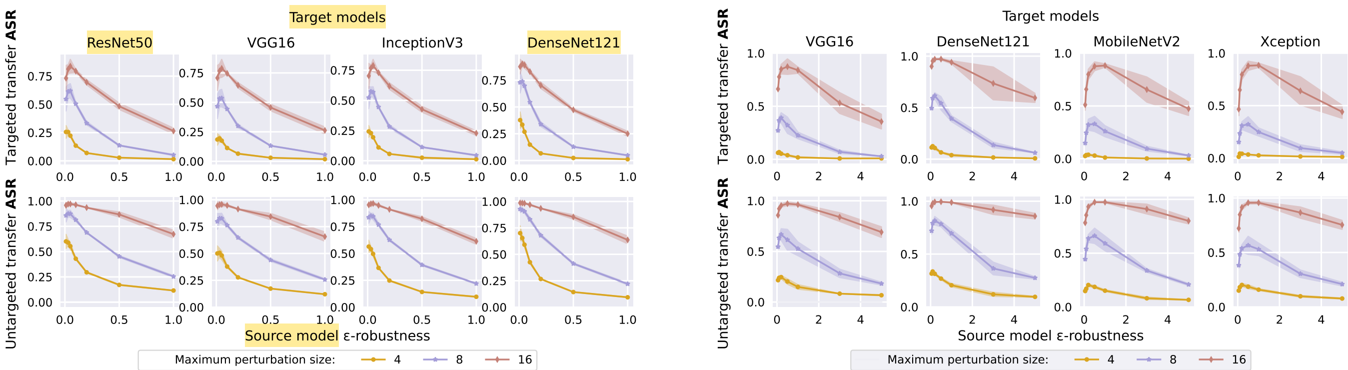

(a) CIFAR-10 (b) ImageNette

Figure 2: Transfer *attack success rates* (**ASRs**) against adversarially trained CIFAR-10 and ImageNette classifiers. We plot the average results of different surrogates obtained by 3 random seeds and the corresponding error bars for each ϵ.

dominant eigenvalue, *and $\nabla_x^2 \ell_{\mathcal{F}}(x, y)$ is the Hessian matrix w.r.t. x. We abbreviate $\sigma_{\mathcal{F},\mathcal{D}}$ as $\sigma_{\mathcal{F}}$ for simplicity and define the upper smoothness as $\overline{\sigma}_{\mathcal{F}} = \sup_{(x,y)\sim\mathcal{D}} \sigma(\nabla_x^2 \ell_{\mathcal{F}}(x, y))$, where $\sup$ is the supremum function.*

A smoother model on $\mathcal{D}$ is featured with smaller $\sigma_{\mathcal{F}}$ and $\overline{\sigma}_{\mathcal{F}}$, indicating more invariance of loss gradient. Different from its original definition where the global Lipschitz constant $\beta_{\mathcal{F}}$ is used [58], we use this curvature metric (*i.e.*, the dominant eigenvalue of the Hessian) to define the model smoothness in a local manner. With this modified definition, we can theoretically and empirically quantify the smoothness of loss surface on $\mathcal{F}$ for a given data distribution $\mathcal{D}$. Moreover, this provides a tighter bound for the model's loss function gradient, namely, an explicit relation $\overline{\sigma}_{\mathcal{F}} \leq \beta_{\mathcal{F}}$ holds. Although the true distribution $\mathcal{D}$ is unknown, one can still sample a set of data from $\mathbf{S}$ and use the empirical mean as an approximation to evaluate the model smoothness. Note that our definition is correlated to the model complexity concept introduced in Demontis *et al.* [5] (see Sec. 6, **Q3**).

Definition 2 (Gradient similarity). *For two models $\mathcal{F}$ and $\mathcal{G}$ with the loss functions $\ell_{\mathcal{F}}$ and $\ell_{\mathcal{G}}$, the gradient similarity over (x, y) is defined as $\mathcal{S}(\ell_{\mathcal{F}}, \ell_{\mathcal{G}}, x, y) = \frac{\nabla_x \ell_{\mathcal{F}}(x,y) \cdot \nabla_x \ell_{\mathcal{G}}(x,y)}{\|\nabla_x \ell_{\mathcal{F}}(x,y)\|_2 \cdot \|\nabla_x \ell_{\mathcal{G}}(x,y)\|_2}$.*

Given a distribution $\mathcal{D}$, we can further define the infimum of loss gradient similarity on $\mathcal{D}$ as $\underline{\mathcal{S}}_{\mathcal{D}}(\ell_{\mathcal{F}}, \ell_{\mathcal{G}}) = \inf_{(x,y)\sim\mathcal{D}} \mathcal{S}(\ell_{\mathcal{F}}, \ell_{\mathcal{G}}, x, y)$. Similar to Demontis *et al.* [5], we define the expected loss gradient similarity as $\tilde{\mathcal{S}}_{\mathcal{D}}(\ell_{\mathcal{F}}, \ell_{\mathcal{G}}) = \mathbb{E}_{(x,y)\sim\mathcal{D}}[\mathcal{S}(\ell_{\mathcal{F}}, \ell_{\mathcal{G}}, x, y)]$, which can capture the similarity between two models on $\mathcal{D}$. Naturally, a larger gradient similarity indicates a more general alignment between the adversarial directions of two given models. We can sample a set of data from $\mathbf{S}$ to evaluate this alignment between two models on $\mathcal{D}$.

Definition 3 (Transferability). *Given a normal sample $(x, y) \in \mathcal{D}$, and a perturbed version $x + \delta$ crafted against a surrogate model $\mathcal{F}$. The transferability T_r between $\mathcal{F}$ and a target model $\mathcal{G}$ is defined as $T_r = \mathbb{I}[\mathcal{F}(x) = \mathcal{G}(x) = y \wedge \mathcal{F}(x + \delta) \neq y \wedge \mathcal{G}(x + \delta) \neq y]$, where $\mathbb{I}$ denotes the indicator function.*

Here we define transferability the same way as [58] for untargeted attacks at the instance level. A successful untargeted transfer attack requires both the surrogate and the target models to give correct predictions for the unperturbed input and incorrect predictions for the perturbed one. The targeted version is similar. Note that we abuse the notations δ and ϵ in Definition 3 and Theorem 1, while the notations in Eq. (1) have similar meanings under different contexts.

Theorem 1 (Lower bound of transferability). *Given any sample $(x, y) \in \mathcal{D}$, let $x + \delta$ denote a perturbed version of x with fooling probability $\Pr(\mathcal{F}(x + \delta) \neq y) \geq (1 - \alpha)$ and perturbation budget $\|\delta\|_2 \leq \epsilon$. Then the transferability $\Pr(T_r(\mathcal{F}, \mathcal{G}, x, y) = 1)$ between surrogate model $\mathcal{F}$ and target model $\mathcal{G}$ can be lower bounded by $\Pr(T_r(\mathcal{F}, \mathcal{G}, x, y) = 1) \geq (1 - \alpha) - (\gamma_{\mathcal{F}} + \gamma_{\mathcal{G}}) - \frac{\epsilon(1+\alpha) - c_{\mathcal{F}}(1-\alpha)}{\epsilon - c_{\mathcal{G}}} - \frac{\epsilon(1-\alpha)}{\epsilon - c_{\mathcal{G}}}\sqrt{2 - 2\underline{\mathcal{S}}_{\mathcal{D}}(\ell_{\mathcal{F}}, \ell_{\mathcal{G}})}$, where*

$$
\begin{aligned}
c_{\mathcal{F}} &= \min_{(x,y)\sim\mathcal{D}} \frac{\min_{y' \in \mathcal{L}: y' \neq y} \ell_{\mathcal{F}}(x + \delta, y') - \ell_{\mathcal{F}}(x, y) - \overline{\sigma}_{\mathcal{F}}\epsilon^2/2}{\|\nabla_x \ell_{\mathcal{F}}(x, y)\|_2}, \\
c_{\mathcal{G}} &= \max_{(x,y)\sim\mathcal{D}} \frac{\min_{y' \in \mathcal{L}: y' \neq y} \ell_{\mathcal{G}}(x + \delta, y') - \ell_{\mathcal{G}}(x, y) + \overline{\sigma}_{\mathcal{G}}\epsilon^2/2}{\|\nabla_x \ell_{\mathcal{G}}(x, y)\|_2}.
\end{aligned}
\tag{2}
$$

The natural risks (inaccuracy) of models $\mathcal{F}$ and $\mathcal{G}$ on $\mathcal{D}$ are defined as $\gamma_{\mathcal{F}}$ and $\gamma_{\mathcal{G}}$ respectively, and $\overline{\sigma}_{\mathcal{F}}$ and $\overline{\sigma}_{\mathcal{G}}$ are the upper smoothness of $\mathcal{F}$ and $\mathcal{G}$.

Note that we deliver the lower bound of transferability for untargeted attacks as an example, and the targeted attack follows a similar form. The conclusions for the targeted attack agree with the untargeted case, as suggested in [58], so we omit it for space. The proof is provided in the Appendix. Although the theorem is initially for l_2-norm perturbations, it can be generalized to l_∞-norm as demonstrated in [58].

Implications. Different from [58], which seeks to suppress the transferability from both surrogate and target sides, this paper focuses on the surrogate aspect alone to increase transferability. Therefore, we next briefly analyze how all

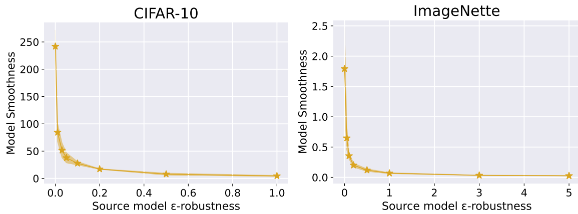

(a) ResNet18 on CIFAR-10 (b) ResNet50 on ImageNette

Figure 3: Average model smoothness of ϵ-robust models trained over 3 different random seeds with corresponding error bars at each ϵ. Note that the variances are very small.

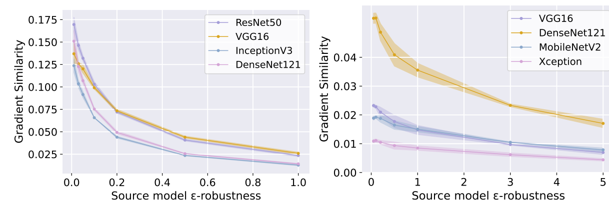

(a) CIFAR-10 (b) ImageNette

Figure 4: Average gradient similarities between ϵ-robust models and different target models with corresponding error bars at each ϵ over 3 different random seeds

the terms relating to $\mathcal{F}$ influence the lower bound.

- **fooling probability** $1-\alpha$: this term captures the likelihood of the surrogate $\mathcal{F}$ being fooled by the adversarial instance $x+\delta$. Different AEs generation strategies result in different fooling probabilities. Intuitively, if $x+\delta$ is unable to fool $\mathcal{F}$, we would expect it cannot fool $\mathcal{G}$ as well. The theorem also suggests effective attack strategies to increase the lower bound. Therefore we default to using a strong baseline attack, *projected gradient descent* (PGD) (Tabs. 2 and 3). Additional, we also AutoAttack (a gradient-based and gradient-free ensemble attack) (Tab. 13) to examine the consistency of conclusions.
- **natural risk** $\gamma_{\mathcal{F}}$: the negative effect of natural risk on the lower bound of transferability is obvious. A model with low accuracy on $\mathcal{D}$ is certainly undesirable for adversarial attacks. Consequently, we minimize this term by training models with sufficient epochs for CIFAR-10 and fine-tuning pre-trained ImageNet classifiers for ImageNette.
- **gradient similarity** $\underline{\mathcal{S}}_{\mathcal{D}}(\ell_{\mathcal{F}},\ell_{\mathcal{G}})$: $\overline{\sigma}_{\mathcal{G}}$ is small compared with the perturbation radius ϵ, and the gradient magnitude $\|\nabla_x \ell_{\mathcal{G}}\|_2$ is relatively large, leading to a small $c_{\mathcal{G}}$. Additionally, $1-\alpha$ is large since the attack is generally effective against $\mathcal{F}$. Thus, the right side of the inequality has a form of $C-k\sqrt{1-\underline{\mathcal{S}}_{\mathcal{D}}(\ell_{\mathcal{F}},\ell_{\mathcal{G}})}$. Since C and k are both positive, there is a positive relationship between gradient similarity and the lower bound.
- **model smoothness** $\overline{\sigma}_{\mathcal{F}}$: It is obvious that a smaller $\overline{\sigma}_{\mathcal{F}}$ generates a larger $c_{\mathcal{F}}$, resulting in a larger lower bound. This indicates smoother models in the input space might serve as better surrogates for transfer attacks.

It is worth noting that a sensible adversary naturally desires to use more precise surrogates and stronger attacks against unknown targets. However, smoothness and similarity are more complex to understand and optimize compared to fooling probability and natural risk. Therefore, we focus on investigating the connection between smoothness, similarity, and transferability as well as how the various training mechanisms regulate them under the restriction that the other two factors above are fairly acceptable. Prior study [5] has shown their link with transferability separately, while we explore their joint effect on transferability.

2.3. Trade-off Under Adversarial Training

Through a combination of theoretical analysis and experimental measurements, here we provide our insights into this "transferability circuit" in adversarial training. Arguably, we make the following two conjectures.

From surrogate's perspective, the trade-off between model smoothness and gradient similarity can significantly indicate adversarial transferability. First, through mathematical derivation and empirical results, we demonstrate that *AT* implicitly improves model smoothness. We rewrite the adversarial loss in Eq. (1) as: $\ell(f(x_i),y_i)+[\max_{\|\delta\|_2<\epsilon}\ell(f(x_i+\delta),y_i)-\ell(f(x_i),y_i)]$. The latter term reflects the non-smoothness around point (x_i,y_i). Assuming x_i is a local minimum of $\ell(f(\cdot),y_i)$ and applying a Taylor expansion, we get $\max_{\|\delta\|_2\leq\epsilon}\ell(f(x_i+\delta),y_i)-\ell(f(x_i),y_i)=\frac{1}{2}\sigma(\nabla x^2\ell(f(x_i),y_i))\cdot\|\delta\|_2^2+O(\|\delta\|_2^3)$ since the first-order term is 0 at a local minimum. Therefore, *AT* implicitly penalizes the curvature of $\ell(f(x_i),y_i)$ with a penalty proportional to the norm of adversarial noise $\|\delta\|_2^2$.

Accordingly, a larger ϵ strengthens the effect of producing models with greater smoothness. Fig. 3 shows the mean dominant eigenvalues of the Hessian for *AT* models under various perturbation budgets. It reveals that *AT* consistently suppresses the dominant eigenvalue, stably producing smoother models. On the other hand, we empirically find that *AT* impairs gradient similarity. Fig. 4 shows the decay of similarity between surrogate and target models as the budget increases. Notably, for each dataset, smoothness rapidly improves for small ϵ (as shown by the steep slope in Fig. 3), while gradient similarity gradually decreases. For larger ϵ, improvements in smoothness become marginal since the models are already very smooth. Recall that we have controlled the other two terms to be reasonably acceptable. These suggest that:

- The quick improvement in transferability for small ϵ occurs could be the cause of the rapid gains in smoothness and small decays in gradient similarity.
- The degradation in transferability for large ϵ occurs may because the smoothness gains have approached the limit while gradient similarity continues to decrease.

Based on the above analyses, we can infer that the "transferability circuit" of *AT* may primarily arise from the trade-off effect between smoothness and similarity, given the restriction of surrogates with relatively good accuracies and a highly effective attack strategy. This inference is intuitively inspired by the implications regarding all the surrogate-related factors in Theorem 1.

TABLE 2: Untargeted and targeted transfer ASRs of AEs crafted against baseline (*ST*), data augmentations, adversarial training, and gradient regularizations surrogates under the different L_∞ budgets (4/255, 8/255, 16/255) on **CIFAR-10** using **PGD**. Results in gray are (more than 0.2%) below the baseline, results in white are close to the baseline ($\pm 0.2\%$). Results in darkest orange are the highest in each respective column, the second darkest are the second highest, and the least dark are others more than 0.2% above the baseline. We conduct experiments using surrogate models trained from 3 different random seeds in each setting and report the average results (in %) and the according error bars.

	4/255				8/255				16/255			
	ResNet50	VGG16	InceptionV3	DenseNet121	ResNet50	VGG16	InceptionV3	DenseNet121	ResNet50	VGG16	InceptionV3	DenseNet121
Untargeted												
ST	$54.3_{\pm 2.9}$	$42.3_{\pm 1.9}$	$53.6_{\pm 2.3}$	$70.7_{\pm 2.0}$	$79.9_{\pm 3.4}$	$71.4_{\pm 3.5}$	$80.1_{\pm 3.2}$	$93.0_{\pm 1.2}$	$92.8_{\pm 1.6}$	$90.6_{\pm 1.9}$	$93.3_{\pm 2.2}$	$98.6_{\pm 0.5}$
MU, $\tau = 1$	$34.7_{\pm 2.6}$	$26.7_{\pm 1.1}$	$35.8_{\pm 1.8}$	$47.1_{\pm 3.0}$	$57.1_{\pm 3.6}$	$49.1_{\pm 2.2}$	$59.2_{\pm 2.6}$	$74.0_{\pm 2.8}$	$76.6_{\pm 4.1}$	$75.2_{\pm 3.4}$	$79.9_{\pm 2.5}$	$90.2_{\pm 2.4}$
MU, $\tau = 5$	$18.5_{\pm 0.5}$	$15.5_{\pm 0.2}$	$19.6_{\pm 0.3}$	$22.8_{\pm 0.5}$	$31.3_{\pm 1.7}$	$27.6_{\pm 0.7}$	$34.5_{\pm 0.7}$	$40.7_{\pm 1.2}$	$49.9_{\pm 1.5}$	$49.1_{\pm 0.9}$	$54.4_{\pm 0.3}$	$62.8_{\pm 1.2}$
CM, $\tau = 1$	$29.3_{\pm 1.2}$	$21.3_{\pm 0.5}$	$28.4_{\pm 2.1}$	$39.8_{\pm 2.0}$	$46.4_{\pm 2.5}$	$37.6_{\pm 1.4}$	$45.6_{\pm 3.2}$	$62.8_{\pm 2.4}$	$63.3_{\pm 2.6}$	$60.2_{\pm 1.4}$	$63.9_{\pm 3.2}$	$81.1_{\pm 1.2}$
CM, $\tau = 5$	$13.5_{\pm 0.3}$	$10.8_{\pm 0.1}$	$13.1_{\pm 0.4}$	$15.1_{\pm 0.3}$	$19.5_{\pm 0.4}$	$15.7_{\pm 0.2}$	$18.7_{\pm 0.8}$	$22.6_{\pm 0.7}$	$29.4_{\pm 1.4}$	$28.6_{\pm 1.0}$	$29.3_{\pm 1.1}$	$34.3_{\pm 1.5}$
CO, $\tau = 1$	$51.5_{\pm 2.3}$	$41.3_{\pm 2.4}$	$50.0_{\pm 1.8}$	$67.7_{\pm 1.4}$	$78.7_{\pm 2.4}$	$71.9_{\pm 3.2}$	$78.2_{\pm 0.9}$	$92.3_{\pm 0.9}$	$93.0_{\pm 2.1}$	$91.8_{\pm 1.5}$	$93.6_{\pm 0.7}$	$98.9_{\pm 0.2}$
CO, $\tau = 5$	$37.7_{\pm 2.8}$	$26.9_{\pm 1.7}$	$36.9_{\pm 2.0}$	$49.5_{\pm 1.2}$	$63.9_{\pm 4.5}$	$53.1_{\pm 3.6}$	$64.1_{\pm 3.9}$	$80.4_{\pm 1.1}$	$84.7_{\pm 3.3}$	$79.1_{\pm 3.5}$	$85.5_{\pm 3.2}$	$95.3_{\pm 1.0}$
LS, $\tau = 1$	$33.4_{\pm 1.7}$	$28.6_{\pm 1.4}$	$33.2_{\pm 0.6}$	$43.4_{\pm 1.5}$	$47.5_{\pm 2.0}$	$44.8_{\pm 1.1}$	$47.6_{\pm 0.8}$	$61.8_{\pm 1.9}$	$59.9_{\pm 1.5}$	$63.0_{\pm 1.1}$	$62.9_{\pm 1.0}$	$75.8_{\pm 1.4}$
LS, $\tau = 5$	$32.8_{\pm 0.5}$	$28.0_{\pm 1.3}$	$31.9_{\pm 0.7}$	$40.8_{\pm 1.8}$	$50.7_{\pm 1.4}$	$46.8_{\pm 2.4}$	$50.6_{\pm 0.6}$	$63.4_{\pm 0.9}$	$65.3_{\pm 2.1}$	$66.1_{\pm 1.9}$	$66.7_{\pm 0.5}$	$78.0_{\pm 0.7}$
AT	$59.0_{\pm 3.0}$	$50.3_{\pm 4.4}$	$53.3_{\pm 2.9}$	$65.3_{\pm 2.7}$	$87.8_{\pm 2.8}$	$82.7_{\pm 4.5}$	$84.7_{\pm 2.7}$	$92.2_{\pm 0.8}$	$96.9_{\pm 1.3}$	$95.8_{\pm 2.0}$	$96.0_{\pm 1.4}$	$98.6_{\pm 0.3}$
IR	$62.3_{\pm 1.2}$	$55.6_{\pm 0.5}$	$56.5_{\pm 2.1}$	$63.7_{\pm 1.9}$	$96.0_{\pm 0.4}$	$93.2_{\pm 0.2}$	$93.8_{\pm 0.6}$	$96.9_{\pm 0.6}$	$99.9_{\pm 0.0}$	$99.7_{\pm 0.0}$	$99.8_{\pm 0.1}$	$99.9_{\pm 0.1}$
JR	$74.2_{\pm 2.0}$	$65.8_{\pm 0.8}$	$72.6_{\pm 0.3}$	$84.1_{\pm 0.5}$	$94.1_{\pm 0.7}$	$91.3_{\pm 0.3}$	$93.4_{\pm 0.6}$	$97.7_{\pm 0.5}$	$98.3_{\pm 0.3}$	$98.3_{\pm 0.2}$	$98.5_{\pm 0.4}$	$99.7_{\pm 0.5}$
ER	$64.9_{\pm 3.3}$	$52.5_{\pm 1.9}$	$54.2_{\pm 6.7}$	$62.8_{\pm 10.9}$	$94.2_{\pm 1.4}$	$87.1_{\pm 5.3}$	$87.9_{\pm 4.7}$	$92.8_{\pm 5.3}$	$99.6_{\pm 0.2}$	$98.7_{\pm 4.0}$	$98.6_{\pm 0.8}$	$99.5_{\pm 0.6}$
SAM	$76.1_{\pm 1.5}$	$64.3_{\pm 2.1}$	$74.5_{\pm 0.7}$	$88.5_{\pm 0.4}$	$97.5_{\pm 0.5}$	$94.1_{\pm 0.8}$	$97.1_{\pm 0.1}$	$99.6_{\pm 0.1}$	$99.8_{\pm 0.0}$	$99.7_{\pm 0.1}$	$99.9_{\pm 0.0}$	$100.0_{\pm 0.0}$
SAM&IR	$64.7_{\pm 0.3}$	$58.2_{\pm 0.4}$	$58.4_{\pm 1.6}$	$65.4_{\pm 1.0}$	$97.6_{\pm 0.0}$	$95.5_{\pm 0.1}$	$95.9_{\pm 0.4}$	$97.9_{\pm 0.3}$	$100.0_{\pm 0.0}$	$99.9_{\pm 0.0}$	$100.0_{\pm 0.0}$	$100.0_{\pm 0.0}$
SAM&JR	$83.1_{\pm 0.6}$	$70.1_{\pm 0.9}$	$79.4_{\pm 0.6}$	$91.5_{\pm 0.3}$	$98.6_{\pm 0.2}$	$96.6_{\pm 0.2}$	$98.3_{\pm 0.1}$	$99.9_{\pm 0.0}$	$99.9_{\pm 0.0}$	$99.9_{\pm 0.0}$	$99.9_{\pm 0.0}$	$100.0_{\pm 0.0}$
Targeted												
ST	$18.3_{\pm 1.4}$	$12.7_{\pm 0.6}$	$20.4_{\pm 1.1}$	$34.9_{\pm 1.9}$	$39.4_{\pm 4.9}$	$32.7_{\pm 3.6}$	$43.6_{\pm 4.0}$	$68.8_{\pm 4.0}$	$55.7_{\pm 6.0}$	$53.5_{\pm 5.5}$	$60.0_{\pm 5.3}$	$85.4_{\pm 4.2}$
MU, $\tau = 1$	$8.2_{\pm 0.8}$	$5.9_{\pm 0.5}$	$10.5_{\pm 0.6}$	$15.9_{\pm 1.0}$	$17.0_{\pm 2.7}$	$13.8_{\pm 1.4}$	$20.7_{\pm 2.1}$	$33.3_{\pm 3.5}$	$28.0_{\pm 5.1}$	$26.8_{\pm 2.9}$	$33.1_{\pm 3.5}$	$50.9_{\pm 6.2}$
MU, $\tau = 5$	$3.0_{\pm 0.1}$	$2.4_{\pm 0.1}$	$4.1_{\pm 0.1}$	$5.0_{\pm 0.2}$	$6.1_{\pm 0.5}$	$5.0_{\pm 0.4}$	$7.9_{\pm 0.5}$	$10.4_{\pm 0.5}$	$10.8_{\pm 0.5}$	$10.7_{\pm 0.6}$	$13.5_{\pm 0.6}$	$16.9_{\pm 0.9}$
CM, $\tau = 1$	$6.0_{\pm 0.4}$	$4.2_{\pm 0.2}$	$6.8_{\pm 1.0}$	$11.4_{\pm 1.1}$	$10.7_{\pm 0.7}$	$8.3_{\pm 0.5}$	$11.6_{\pm 1.8}$	$20.8_{\pm 1.9}$	$16.4_{\pm 0.9}$	$14.9_{\pm 0.8}$	$17.3_{\pm 2.5}$	$29.6_{\pm 1.7}$
CM, $\tau = 5$	$2.0_{\pm 0.1}$	$1.6_{\pm 0.1}$	$2.4_{\pm 0.2}$	$2.8_{\pm 0.2}$	$2.8_{\pm 0.1}$	$2.3_{\pm 0.0}$	$3.2_{\pm 0.1}$	$3.7_{\pm 0.1}$	$4.2_{\pm 0.2}$	$3.9_{\pm 0.4}$	$4.4_{\pm 0.2}$	$4.7_{\pm 0.3}$
CO, $\tau = 1$	$16.0_{\pm 1.3}$	$11.3_{\pm 1.2}$	$17.6_{\pm 1.1}$	$30.6_{\pm 1.7}$	$35.8_{\pm 3.0}$	$30.7_{\pm 2.5}$	$38.6_{\pm 2.7}$	$63.4_{\pm 2.2}$	$52.8_{\pm 4.3}$	$51.5_{\pm 3.0}$	$55.9_{\pm 3.1}$	$82.1_{\pm 1.6}$
CO, $\tau = 5$	$7.9_{\pm 1.1}$	$5.4_{\pm 0.5}$	$9.5_{\pm 0.7}$	$14.2_{\pm 0.7}$	$17.4_{\pm 2.9}$	$13.6_{\pm 1.3}$	$20.5_{\pm 2.1}$	$31.1_{\pm 0.9}$	$29.1_{\pm 5.0}$	$24.9_{\pm 2.8}$	$31.9_{\pm 4.1}$	$48.5_{\pm 1.8}$
LS, $\tau = 1$	$6.8_{\pm 0.6}$	$5.4_{\pm 0.4}$	$7.0_{\pm 0.3}$	$10.7_{\pm 1.3}$	$9.9_{\pm 3.8}$	$9.0_{\pm 4.0}$	$10.0_{\pm 3.3}$	$15.6_{\pm 6.2}$	$15.4_{\pm 1.9}$	$16.7_{\pm 1.8}$	$16.3_{\pm 1.2}$	$23.9_{\pm 2.9}$
LS, $\tau = 5$	$6.7_{\pm 0.4}$	$5.7_{\pm 0.1}$	$7.1_{\pm 0.8}$	$10.5_{\pm 1.3}$	$13.5_{\pm 1.1}$	$12.8_{\pm 0.7}$	$14.0_{\pm 1.5}$	$20.1_{\pm 2.0}$	$19.4_{\pm 0.9}$	$20.0_{\pm 0.3}$	$20.0_{\pm 1.4}$	$27.0_{\pm 1.8}$
AT	$24.9_{\pm 2.2}$	$18.6_{\pm 3.4}$	$21.9_{\pm 2.0}$	$32.5_{\pm 2.5}$	$60.7_{\pm 6.7}$	$52.4_{\pm 7.9}$	$55.6_{\pm 5.5}$	$72.6_{\pm 4.0}$	$77.4_{\pm 7.7}$	$74.6_{\pm 7.9}$	$72.4_{\pm 6.7}$	$88.4_{\pm 4.1}$
IR	$25.7_{\pm 1.1}$	$20.6_{\pm 0.2}$	$22.5_{\pm 1.1}$	$28.8_{\pm 1.3}$	$70.8_{\pm 0.5}$	$62.8_{\pm 0.7}$	$65.0_{\pm 1.5}$	$75.2_{\pm 0.6}$	$89.9_{\pm 0.7}$	$86.7_{\pm 0.8}$	$86.3_{\pm 1.3}$	$92.7_{\pm 0.8}$
JR	$38.6_{\pm 2.6}$	$30.3_{\pm 1.2}$	$39.1_{\pm 0.1}$	$54.0_{\pm 1.2}$	$75.2_{\pm 3.9}$	$69.6_{\pm 2.5}$	$76.0_{\pm 0.9}$	$90.0_{\pm 0.8}$	$87.3_{\pm 2.8}$	$88.9_{\pm 1.8}$	$88.4_{\pm 1.0}$	$97.6_{\pm 0.3}$
ER	$22.7_{\pm 1.6}$	$15.5_{\pm 2.8}$	$17.8_{\pm 3.4}$	$24.1_{\pm 8.1}$	$54.6_{\pm 3.3}$	$42.7_{\pm 6.9}$	$44.1_{\pm 8.0}$	$55.0_{\pm 15.9}$	$77.2_{\pm 3.0}$	$67.2_{\pm 8.3}$	$66.5_{\pm 9.6}$	$76.6_{\pm 16.7}$
SAM	$35.0_{\pm 1.9}$	$25.2_{\pm 1.8}$	$36.9_{\pm 1.3}$	$56.7_{\pm 0.2}$	$74.7_{\pm 3.1}$	$65.7_{\pm 3.5}$	$76.5_{\pm 1.9}$	$94.0_{\pm 0.4}$	$92.3_{\pm 1.5}$	$90.9_{\pm 2.2}$	$93.4_{\pm 0.3}$	$99.5_{\pm 0.2}$
SAM&IR	$28.6_{\pm 0.2}$	$23.5_{\pm 0.2}$	$25.0_{\pm 1.2}$	$31.4_{\pm 0.7}$	$81.8_{\pm 0.0}$	$75.7_{\pm 0.2}$	$77.6_{\pm 1.1}$	$84.8_{\pm 0.6}$	$99.2_{\pm 0.1}$	$98.7_{\pm 0.1}$	$98.6_{\pm 0.4}$	$99.6_{\pm 0.1}$
SAM&JR	$44.2_{\pm 1.5}$	$32.9_{\pm 1.1}$	$46.1_{\pm 1.3}$	$65.7_{\pm 0.3}$	$85.5_{\pm 1.4}$	$77.6_{\pm 1.7}$	$87.3_{\pm 1.4}$	$97.6_{\pm 0.1}$	$98.3_{\pm 0.5}$	$97.5_{\pm 0.4}$	$98.6_{\pm 0.4}$	$99.9_{\pm 0.0}$

Meanwhile, we observe that though the "transferability circuit" of *AT* generally exists, it varies under different non-surrogate circumstances. For example, the optimal ϵ AT to achieve the best ASRs varies among datasets and perturbation budgets in Fig. 2. This suggests that for different non-surrogate factors, the extent to which model smoothness and gradient similarity contribute to transferability may vary.

Consequently, we propose the conjecture that the trade-off between smoothness and similarity has a significant correlation with the transferability of AEs when generating them against accurate surrogate models using effective strategies. To validate this conjecture, we will investigate the variations in smoothness, similarity, and the corresponding transfer ASRs under various surrogate training mechanisms in Secs. 3 and 4. Furthermore, in Sec. 6, **Q1**, we provide a statistical analysis of the correlations among model smoothness, gradient similarity, and transferability. Moving forward, the primary concern at hand is to ascertain the rationale of this similarity deterioration in *AT*, as well as how to generally avoid this and reach a better balance of smoothness and similarity for stronger transfer attacks.

Data distribution shift impairs gradient similarity. Different from model smoothness, it is difficult to understand how exactly *AT* degrades the gradient similarity. In this work, we attribute the degradation to the data distribution shift induced by the off-manifold examples in *AT*. Since the emerging of adversarial examples [48], there is a long-held belief that: *Clean data lies in a low-dimensional manifold. Even though the adversarial examples are close to the clean data, they lie off the underlying data manifold* [15, 29, 43]. Nevertheless, recent researches demonstrate that AEs can also be on-manifold [23, 27, 37, 46], and on-manifold and off-manifold AEs may co-exist [55]. With this in mind, we analyze how *AT* enlarges the data distribution shift along with the increment of adversarial budget ϵ.

Given a regular loss function $\ell(f(x), y)$ on the low-dimensional manifold $\mathcal{M}$, the adversarial perturbation $\delta \in \mathbb{R}^d$ could make the loss $\ell(f(x+\delta), y)$ sufficiently high with $x+\delta \in \mathcal{M}$ or $x+\delta \notin \mathcal{M}$ [57]. At a high level, *AT* augments the dataset by adding adversarial samples during each iteration, obtaining an augmented data distribution on $\mathcal{P}_\mathcal{X}$, and the adversarial budget ϵ can be regarded as a parameter that controls the augmentation magnitude. Intuitively, a larger ϵ induces a larger distribution shift, resulting in more space for off-manifold samples. Accordingly, a larger ϵ may cause more disbenefit of underfitting to normal $\mathcal{M}$. We formalize

TABLE 3: Transfer ASRs (in %) of AEs on **ImageNette** using **PGD**. We plot this table in the same way as Tab. 2.

	4/255				8/255				16/255			
	VGG16	DenseNet121	MobileNetV2	Xception	VGG16	DenseNet121	MobileNetV2	Xception	VGG16	DenseNet121	MobileNetV2	Xception
Untargeted												
ST	$11.2_{\pm1.0}$	$17.5_{\pm1.1}$	$7.6_{\pm0.4}$	$8.7_{\pm0.5}$	$28.7_{\pm1.1}$	$42.7_{\pm3.5}$	$18.3_{\pm0.7}$	$18.5_{\pm1.3}$	$61.7_{\pm4.7}$	$81.4_{\pm4.6}$	$49.3_{\pm2.7}$	$44.1_{\pm5.1}$
MU, $\tau=1$	$9.2_{\pm1.6}$	$12.7_{\pm0.9}$	$7.2_{\pm0.6}$	$7.2_{\pm0.2}$	$20.7_{\pm1.3}$	$22.7_{\pm1.3}$	$13.7_{\pm1.5}$	$12.7_{\pm1.1}$	$43.9_{\pm2.3}$	$53.3_{\pm4.1}$	$38.3_{\pm3.1}$	$29.3_{\pm2.9}$
MU, $\tau=5$	$6.7_{\pm1.1}$	$6.7_{\pm0.9}$	$5.1_{\pm0.5}$	$5.7_{\pm0.5}$	$11.5_{\pm0.5}$	$12.0_{\pm0.6}$	$8.1_{\pm0.7}$	$8.1_{\pm0.1}$	$29.3_{\pm0.7}$	$29.2_{\pm2.4}$	$24.1_{\pm1.3}$	$18.8_{\pm0.2}$
CM, $\tau=1$	$7.8_{\pm0.6}$	$10.6_{\pm1.0}$	$6.1_{\pm0.7}$	$7.1_{\pm0.5}$	$16.5_{\pm1.3}$	$18.1_{\pm1.7}$	$10.3_{\pm0.3}$	$10.3_{\pm0.1}$	$35.8_{\pm1.0}$	$42.6_{\pm2.4}$	$29.6_{\pm2.0}$	$21.5_{\pm0.5}$
CM, $\tau=5$	$5.5_{\pm0.5}$	$6.3_{\pm0.1}$	$4.2_{\pm0.4}$	$4.6_{\pm0.4}$	$8.9_{\pm0.9}$	$9.3_{\pm0.3}$	$6.7_{\pm0.3}$	$6.7_{\pm0.5}$	$19.3_{\pm0.5}$	$18.3_{\pm1.1}$	$17.0_{\pm0.6}$	$11.7_{\pm0.5}$
CO, $\tau=1$	$11.8_{\pm0.4}$	$16.7_{\pm1.1}$	$8.1_{\pm0.5}$	$8.7_{\pm0.3}$	$28.3_{\pm1.1}$	$40.5_{\pm2.9}$	$18.5_{\pm0.7}$	$18.4_{\pm1.4}$	$61.8_{\pm1.4}$	$79.8_{\pm2.4}$	$50.9_{\pm1.9}$	$43.8_{\pm0.6}$
CO, $\tau=5$	$10.3_{\pm0.7}$	$14.3_{\pm0.3}$	$7.3_{\pm0.9}$	$7.7_{\pm0.7}$	$25.1_{\pm1.7}$	$34.5_{\pm2.3}$	$17.3_{\pm1.9}$	$15.9_{\pm1.1}$	$56.4_{\pm4.2}$	$75.0_{\pm3.6}$	$46.3_{\pm0.9}$	$40.1_{\pm2.1}$
LS, $\tau=1$	$6.8_{\pm0.6}$	$8.7_{\pm0.3}$	$5.2_{\pm0.4}$	$5.9_{\pm0.9}$	$13.2_{\pm0.6}$	$14.7_{\pm0.1}$	$9.5_{\pm0.1}$	$8.5_{\pm0.5}$	$27.6_{\pm0.2}$	$35.5_{\pm0.7}$	$24.8_{\pm0.8}$	$18.0_{\pm0.6}$
LS, $\tau=5$	$6.1_{\pm0.3}$	$7.1_{\pm0.5}$	$4.7_{\pm0.5}$	$5.5_{\pm0.5}$	$9.1_{\pm1.1}$	$10.2_{\pm0.8}$	$7.2_{\pm0.2}$	$7.8_{\pm0.2}$	$20.0_{\pm1.2}$	$23.1_{\pm1.3}$	$18.6_{\pm1.6}$	$14.4_{\pm0.8}$
AT	$14.7_{\pm2.1}$	$20.5_{\pm1.5}$	$15.3_{\pm1.3}$	$15.7_{\pm0.9}$	$52.1_{\pm6.3}$	$68.7_{\pm2.9}$	$59.3_{\pm7.1}$	$52.3_{\pm5.1}$	$96.5_{\pm1.5}$	$98.8_{\pm0.4}$	$97.5_{\pm0.5}$	$95.7_{\pm0.9}$
IR	$21.0_{\pm6.6}$	$31.7_{\pm6.9}$	$18.5_{\pm5.1}$	$19.5_{\pm4.3}$	$62.5_{\pm14.3}$	$85.6_{\pm9.0}$	$65.2_{\pm16.4}$	$58.4_{\pm14.0}$	$94.7_{\pm6.9}$	$99.5_{\pm0.3}$	$95.7_{\pm5.3}$	$94.6_{\pm5.0}$
JR	$26.3_{\pm2.1}$	$37.3_{\pm0.7}$	$21.7_{\pm1.3}$	$20.5_{\pm1.3}$	$68.5_{\pm2.1}$	$87.0_{\pm0.2}$	$67.6_{\pm3.6}$	$56.0_{\pm5.6}$	$95.0_{\pm1.4}$	$99.5_{\pm0.1}$	$94.7_{\pm1.1}$	$89.8_{\pm3.0}$
ER	$13.2_{\pm2.8}$	$20.9_{\pm1.7}$	$8.9_{\pm1.5}$	$9.6_{\pm1.0}$	$33.3_{\pm9.9}$	$51.1_{\pm8.7}$	$20.7_{\pm3.7}$	$20.5_{\pm3.3}$	$67.5_{\pm15.9}$	$89.3_{\pm6.7}$	$54.5_{\pm9.1}$	$50.1_{\pm8.7}$
SAM	$22.8_{\pm1.4}$	$29.7_{\pm1.5}$	$12.8_{\pm0.8}$	$12.8_{\pm0.0}$	$58.7_{\pm2.7}$	$72.8_{\pm2.0}$	$42.3_{\pm1.1}$	$34.7_{\pm1.7}$	$91.4_{\pm2.0}$	$97.1_{\pm0.3}$	$81.0_{\pm1.8}$	$75.3_{\pm1.7}$
SAM&IR	$26.9_{\pm5.5}$	$39.8_{\pm4.8}$	$24.3_{\pm4.7}$	$23.2_{\pm4.0}$	$72.5_{\pm10.9}$	$92.6_{\pm2.8}$	$78.5_{\pm9.5}$	$68.9_{\pm10.3}$	$98.1_{\pm2.1}$	$99.8_{\pm0.2}$	$98.7_{\pm1.5}$	$97.7_{\pm2.3}$
SAM&JR	$32.7_{\pm4.3}$	$46.3_{\pm3.7}$	$28.1_{\pm4.5}$	$24.9_{\pm4.1}$	$76.6_{\pm5.6}$	$93.6_{\pm1.2}$	$73.1_{\pm7.7}$	$65.9_{\pm7.7}$	$96.7_{\pm7.3}$	$99.8_{\pm0.2}$	$96.6_{\pm1.6}$	$93.9_{\pm4.1}$
Targeted												
ST	$2.1_{\pm0.3}$	$4.1_{\pm0.3}$	$0.6_{\pm0.4}$	$2.0_{\pm0.2}$	$10.4_{\pm0.8}$	$19.6_{\pm2.8}$	$4.2_{\pm0.4}$	$5.7_{\pm1.7}$	$33.6_{\pm3.8}$	$60.3_{\pm7.5}$	$19.5_{\pm2.1}$	$19.7_{\pm3.1}$
MU, $\tau=1$	$1.3_{\pm0.3}$	$2.3_{\pm0.3}$	$0.4_{\pm0.2}$	$1.0_{\pm0.2}$	$5.1_{\pm0.7}$	$7.3_{\pm1.1}$	$1.5_{\pm0.3}$	$2.5_{\pm0.1}$	$15.7_{\pm1.9}$	$25.1_{\pm4.1}$	$9.3_{\pm1.5}$	$8.8_{\pm2.4}$
MU, $\tau=5$	$0.9_{\pm0.1}$	$0.6_{\pm0.0}$	$0.1_{\pm0.1}$	$0.5_{\pm0.1}$	$1.3_{\pm0.3}$	$1.1_{\pm0.1}$	$0.4_{\pm0.4}$	$1.0_{\pm0.2}$	$3.8_{\pm0.8}$	$3.7_{\pm0.7}$	$1.7_{\pm0.1}$	$2.8_{\pm0.6}$
CM, $\tau=1$	$1.1_{\pm0.5}$	$1.4_{\pm0.2}$	$0.2_{\pm0.2}$	$0.7_{\pm0.3}$	$2.3_{\pm0.3}$	$3.1_{\pm0.5}$	$0.7_{\pm0.1}$	$1.7_{\pm0.5}$	$6.5_{\pm0.5}$	$9.4_{\pm0.4}$	$3.7_{\pm0.3}$	$4.9_{\pm0.3}$
CM, $\tau=5$	$0.7_{\pm0.1}$	$0.8_{\pm0.0}$	$0.1_{\pm0.1}$	$0.4_{\pm0.2}$	$0.9_{\pm0.3}$	$1.0_{\pm0.2}$	$0.2_{\pm0.2}$	$0.9_{\pm0.1}$	$2.3_{\pm0.3}$	$2.5_{\pm0.1}$	$1.4_{\pm0.4}$	$1.6_{\pm0.2}$
CO, $\tau=1$	$2.3_{\pm0.5}$	$3.4_{\pm0.6}$	$0.4_{\pm0.2}$	$1.7_{\pm0.3}$	$9.3_{\pm1.3}$	$18.2_{\pm3.0}$	$3.2_{\pm1.0}$	$4.9_{\pm0.5}$	$31.0_{\pm2.4}$	$62.3_{\pm6.9}$	$18.2_{\pm1.6}$	$17.4_{\pm1.8}$
CO, $\tau=5$	$1.9_{\pm0.1}$	$3.1_{\pm0.9}$	$0.6_{\pm0.2}$	$1.2_{\pm0.2}$	$8.8_{\pm1.4}$	$14.9_{\pm0.9}$	$3.8_{\pm1.0}$	$4.3_{\pm1.1}$	$28.3_{\pm2.9}$	$52.5_{\pm2.1}$	$16.2_{\pm3.0}$	$16.9_{\pm1.3}$
LS, $\tau=1$	$0.9_{\pm0.1}$	$1.5_{\pm0.5}$	$0.4_{\pm0.0}$	$0.7_{\pm0.1}$	$1.6_{\pm0.0}$	$2.5_{\pm0.1}$	$0.5_{\pm0.1}$	$1.4_{\pm0.2}$	$4.0_{\pm0.2}$	$6.3_{\pm0.7}$	$3.2_{\pm0.6}$	$2.8_{\pm0.2}$
LS, $\tau=5$	$0.7_{\pm0.1}$	$1.2_{\pm0.0}$	$0.3_{\pm0.1}$	$0.5_{\pm0.3}$	$1.2_{\pm0.0}$	$1.9_{\pm0.5}$	$0.3_{\pm0.1}$	$1.0_{\pm0.2}$	$2.7_{\pm0.9}$	$3.7_{\pm0.9}$	$2.2_{\pm0.4}$	$2.3_{\pm0.7}$
AT	$2.1_{\pm0.9}$	$4.0_{\pm0.8}$	$1.1_{\pm0.3}$	$2.6_{\pm0.2}$	$22.5_{\pm3.1}$	$39.3_{\pm2.9}$	$26.2_{\pm5.4}$	$25.1_{\pm4.1}$	$84.7_{\pm3.7}$	$94.1_{\pm1.5}$	$88.3_{\pm2.2}$	$89.3_{\pm2.5}$
IR	$4.2_{\pm2.0}$	$9.9_{\pm3.7}$	$3.4_{\pm1.6}$	$3.3_{\pm1.1}$	$33.6_{\pm13.4}$	$65.3_{\pm14.3}$	$34.1_{\pm12.7}$	$31.9_{\pm13.5}$	$84.5_{\pm14.3}$	$98.2_{\pm2.2}$	$86.9_{\pm12.3}$	$84.6_{\pm14.6}$
JR	$6.5_{\pm0.5}$	$14.0_{\pm0.8}$	$4.6_{\pm0.4}$	$4.8_{\pm0.6}$	$41.4_{\pm5.2}$	$71.7_{\pm2.5}$	$36.5_{\pm5.7}$	$33.6_{\pm5.8}$	$82.5_{\pm7.3}$	$98.1_{\pm1.3}$	$79.5_{\pm6.7}$	$76.0_{\pm9.4}$
ER	$2.6_{\pm0.8}$	$5.9_{\pm1.5}$	$0.7_{\pm0.3}$	$1.9_{\pm0.3}$	$12.3_{\pm5.7}$	$26.7_{\pm8.1}$	$4.7_{\pm1.5}$	$6.7_{\pm2.5}$	$40.4_{\pm20.8}$	$75.0_{\pm12.8}$	$23.5_{\pm9.9}$	$24.6_{\pm10.8}$
SAM	$6.1_{\pm1.1}$	$8.9_{\pm0.9}$	$2.3_{\pm0.5}$	$3.3_{\pm0.1}$	$28.1_{\pm1.1}$	$46.5_{\pm1.3}$	$12.6_{\pm2.0}$	$11.6_{\pm0.8}$	$76.0_{\pm0.4}$	$92.1_{\pm1.1}$	$52.4_{\pm1.0}$	$53.7_{\pm1.3}$
SAM&IR	$5.9_{\pm2.1}$	$13.2_{\pm2.8}$	$5.2_{\pm1.6}$	$4.3_{\pm0.9}$	$44.2_{\pm12.8}$	$76.3_{\pm4.5}$	$46.5_{\pm12.1}$	$43.6_{\pm11.8}$	$92.5_{\pm6.7}$	$99.5_{\pm0.1}$	$93.5_{\pm4.5}$	$92.4_{\pm4.8}$
SAM&JR	$9.9_{\pm1.3}$	$19.5_{\pm1.3}$	$6.4_{\pm0.6}$	$5.9_{\pm1.1}$	$50.0_{\pm6.4}$	$78.7_{\pm1.7}$	$41.4_{\pm9.0}$	$38.4_{\pm7.2}$	$88.7_{\pm7.5}$	$99.3_{\pm0.1}$	$83.1_{\pm5.7}$	$84.1_{\pm7.1}$

this as follows:

Hypothesis 1 (Distribution shift impairs gradient similarity). *Given two data distribution $\mathcal{D}, \mathcal{D}' \in \mathcal{P}_{\mathcal{X}\times\mathcal{Y}}$, and two source models $\mathcal{F}_{\mathcal{D}}$ and $\mathcal{F}_{\mathcal{D}'}$ trained on $\mathcal{D}$ and $\mathcal{D}'$, respectively, supposing the target model $\mathcal{G}_{\mathcal{D}}$ is also trained on $\mathcal{D}$ and they all share a joint training loss ℓ, if the distance between $\mathcal{D}$ and $\mathcal{D}'$ is large enough, then $\tilde{\mathcal{S}}_{\mathcal{D}}\left(\ell_{\mathcal{F}_{\mathcal{D}'}}, \ell_{\mathcal{G}_{\mathcal{D}}}\right) < \tilde{\mathcal{S}}_{\mathcal{D}}\left(\ell_{\mathcal{F}_{\mathcal{D}}}, \ell_{\mathcal{G}_{\mathcal{D}}}\right)$ is likely to stand.*

The intuition behind this hypothesis is that, on average, the two models trained on the same distribution should align better in the gradient direction than those trained with different distributions. Note that, we relax the distribution change of *AT* on $\mathcal{P}_{\mathcal{X}}$ to $\mathcal{P}_{\mathcal{X}\times\mathcal{Y}}$ here, hypothesizing the general change on $\mathcal{P}_{\mathcal{X}\times\mathcal{Y}}$ impairs gradient similarity.

3. Investigating Data Augmentation

To extend the distribution shifts of *AT* to more general cases and further verify Hypothesis 1, we investigate how data augmentations, the popular training paradigm that explicitly changes data distribution, influence gradient similarity. Additionally, we investigate the trade-off effect between similarity and smoothness under data augmentations and observe how they reflect on the transfer attack accordingly.

3.1. Data Augmentation Mechanisms

We explore 4 popular data augmentation mechanisms and choose proper augmentation magnitude parameters to control the degree of data distribution shift from $\mathcal{D}$ to $\mathcal{D}'$, aligning the augmentation parameter ϵ in *AT*.

Mixup (*MU*) [61] trains a model on the convex combination of randomly selected sample pairs, *i.e.*, the mixed image $\tilde{x}_{i,j} = bx_i + (1-b)x_j$ and the corresponding label $\tilde{y}_{i,j} = by_i + (1-b)y_j$, where $(x_i, y_i), (x_j, y_j) \in \mathbf{S}$. Here $b \in [0,1]$ is a random variable drawn from the Beta distribution $\mathrm{Beta}(1,1)$. Additionally, we use a probability parameter $\mathbf{p}$ to control how much $\mathcal{D}'$ shifts away from $\mathcal{D}$. Specifically, as $\mathbf{p} \to 0$, the augmented dataset will be identical to $\mathbf{S}$; as $\mathbf{p} \to 1$, all the samples will be interpolated. We train augmented models for *MU* with $\mathbf{p} \in [0.1, 0.3, 0.5, 0.7, 0.9]$.

Cutmix (*CM*) [60] also augments both images and labels by mixing samples. The difference is patches are cut and pasted among training samples. A mixed sample $\tilde{x}_{i,j} = \mathbf{M_b} \odot x_i + (\mathbf{1} - \mathbf{M_b}) \odot x_j$ and its label $\tilde{y}_{i,j}$ are also obtained from two samples $(x_i, y_i), (x_j, y_j) \in \mathbf{S}$, where $\mathbf{M_b}$ is a binary matrix with the same size of x_i to indicate the location for cutting and pasting, $\mathbf{1}$ is a matrix filled with 1, and b is drawn from $\mathrm{Beta}(1,1)$. Similar to *MU*, we use a probability parameter $\mathbf{p}$ to control the augmentation magnitude and train augmented models for *CM* with $\mathbf{p} \in [0.1, 0.3, 0.5, 0.7, 0.9]$.

Cutout (*CO*) [6] augments the dataset by masking out random regions of images with a size less than $M \times M$. In the real implementation, the mask-out region and its size for each image are not deterministic. A bigger M value indicates it is more likely to mask out a bigger region. Hence, we utilize the value of M only to regulate the extent of augmentation since it probabilistically governs the augmentation magnitude, similar to the role of $\mathbf{p}$ in *MU* and *CM*. We select $M \in [8, 12, 16, 20, 24]$ and $M \in [80, 100, 120, 140, 160]$ for CIFAR-10 and ImageNette, respectively.

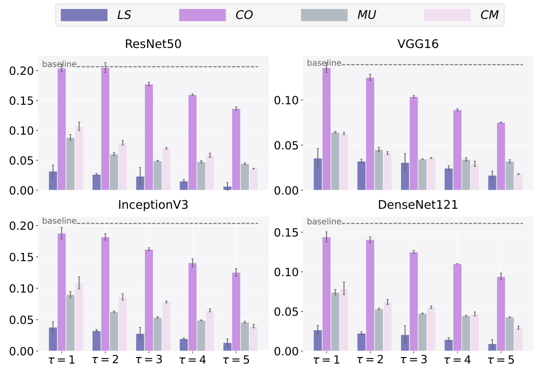

Figure 5: Gradient similarities between augmented surrogate and *ST* target CIFAR-10 models with error bars at each τ

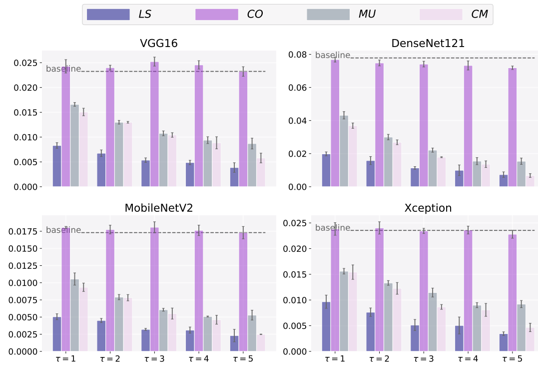

Figure 6: Gradient similarities between augmented surrogate and *ST* target ImageNette models with error bars at each τ

Label smoothing (*LS*) [47] augments the dataset by replacing the hard labels $\mathcal{L}$ with soft continuous labels in probability distribution. Specifically, the probability of the ground-truth class is $1-p$, and the probability of other classes will be uniformly assigned to $p/(m-1)$, where p is chosen from $[0,1)$ and m denotes the number of classes. We train models for *LS* with $p \in [0.1, 0.2, 0.3, 0, 4, 0.5]$.

These augmentations along with *AT* change data distributions in distinct manners. For a normal sample $(x,y) \sim \mathcal{D}$, *AT* associates input feature x with ground-truth y "inaccurately" under a noise δ, while *CO* associates part of "right" x with ground-truth y, thus they explicitly change the distribution on $\mathcal{P}_{\mathcal{X}}$. Contrarily, both *MU* and *CM* correlate parts of x with y, causing shift in $\mathcal{P}_{\mathcal{X}\times\mathcal{Y}}$, whereas *LS* relates the full x to a "wrong" y', causing shift in $\mathcal{P}_{\mathcal{Y}}$. Intuitively, these augmentation methods will cause different impacts on the gradient $\nabla \ell_{\mathcal{F}}(x,y)$. As we select 5 augmentation magnitudes for each augmentation, we use a general parameter $\tau \in [1,2,3,4,5]$ to simplify the notations, *e.g.*, $\tau = 1$ means $\mathbf{p} = 0.1$ for *MU* and $M = 8$ for *CO* on CIFAR-10.

3.2. Data Augmentation Impairs Similarity

To verify Hypothesis 1, we explore how different data distribution shifts influence gradient similarity. For all the experiments, we train models with 3 different random seeds in each setting. Besides, multiple target models are considered to ensure generality. The results over 3 standard training (*ST*) models without augmentations are used as baselines.

Figs. 5 and 6 depict the alignments towards multiple target models for CIFAR-10 and ImageNette. First, we observe that *CO* harms gradient similarity the least, but its effect varies across different datasets. Specifically, *CO* slightly degrades gradient similarity in CIFAR-10 while appearing comparable to baselines in ImageNette. The difference in training settings between the two datasets could be the reason for this gap; CIFAR-10 models are trained from scratch, while ImageNette models are obtained by fine-tuning well-trained ImageNet classifiers. These different outcomes suggest that simply removing some pixels is not enough to make the model forget what it has previously "seen", since ImageNette is a 10-class subset of ImageNet. On the other hand, *LS*, *MU*, and *CM* degrade similarity largely over both datasets. Note that the similarity degradations of these augmentations are in line with their manipulations on $\mathcal{P}_{\mathcal{Y}}$, suggesting modifying the ground-truth y during training results in more impacts on the direction of gradient $\nabla \ell_{\mathcal{F}}(x,y)$. In summary, despite subtle differences, **the results on both datasets support the hypothesis that data distribution shift impairs gradient similarity. Further, the distribution shift in $\mathcal{P}_{\mathcal{Y}}$ may have a greater negative impact on similarity than that in $\mathcal{P}_{\mathcal{X}}$.**

3.3. Trade-off Under Data Augmentation

To figure out how these augmentations influence smoothness and transferability, we measure smoothness and the ASRs of AEs *w.r.t.* these augmented models. To save space, we merely report the $\tau = 1, 5$ cases for PGD attack in Tabs. 2 and 3, as they represent the smallest and largest augmentation magnitudes. We report the $\tau = 1, 3, 5$ cases for AutoAttack in Tab. 13. Figs. 7 and 8 plots the smoothness for augmented models on two datasets.

First, *LS* exhibits a monotonous benefit on smoothness on both datasets due to its implicit effect on reducing the gradient norm during training [47]. However, the tables show that the ASRs of *LS* are always lower than those of *ST*, implying this benefit may not completely offset the negative effect of largely degraded similarity in *LS*. Additionally, there is no monotonicity in ASRs in *LS*, aligning with the always combating negative and positive effects. In contrast, other augmentations do not exhibit a consistent tendency for smoothness on both datasets. Specifically, in CIFAR-10, *CM*, *MU*, and *CO* mostly degrade the smoothness while the degradation is not strictly monotonous. The situation is even more chaotic in ImageNette, where the variances of smoothness are relatively large. However, the ASRs do reveal some patterns. For *CM* and *MU*, their ASRs degrade from $\tau = 1$ to $\tau = 5$, and the ASRs of *CO* are generally better than *MU* and *CM*. Notably, *CO* performs slightly better than *ST* under a few cases, especially when $\tau = 1$. This agrees with the fact that *CO* has slightly better smoothness and less severely degraded similarity. Conclusively, **the trade-off under data augmentations is quite complex, and no single augmentation can produce good surrogates**.

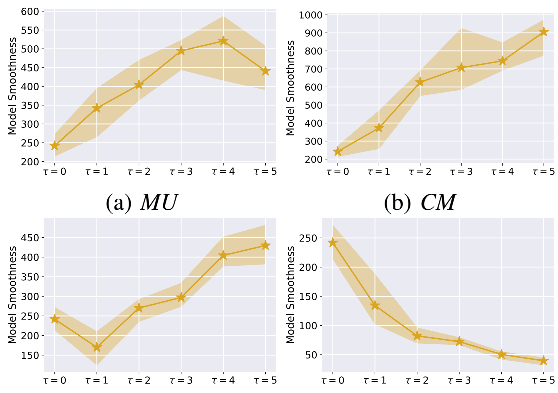

(a) *MU* (b) *CM*

(c) *CO* (d) *LS*

Figure 7: Average model smoothness of augmented models on CIFAR-10 with respective error bars at each τ

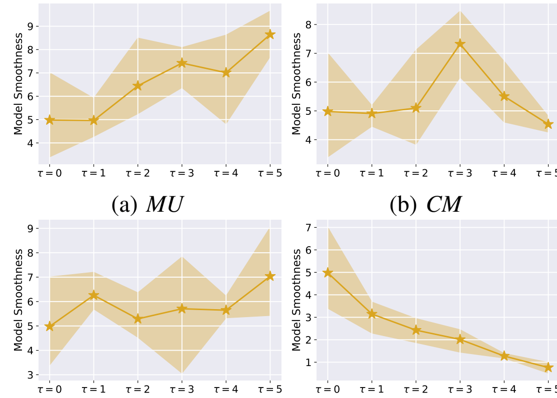

(a) *MU* (b) *CM*

(c) *CO* (d) *LS*

Figure 8: Average model smoothness of augmented models on ImageNette with respective error bars at each τ

4. Investigating Gradient Regularization

At present, we recognize what may harm gradient similarity, but have no idea of how to generally improve it. Additionally, it is challenging to regulate similarity independently without affecting other factors, especially in black-box scenarios where target models are unknown. In contrast, the standalone model smoothness can be regulated and measured with the surrogate itself. Therefore, we will explore how gradient regularization, which is expected to improve smoothness without changing the data distribution, can be used to enhance surrogates.

4.1. Gradient Regularization Mechanisms

We first formally define gradient regularization and deliver the intuitions on why they are chosen. To sharpen the analysis, we introduce the notation θ to parameterize a neural network and reform $f(\cdot)$ as $f_\theta(\cdot)$ if needed. For concise illustrations, we sometimes abbreviate $l(f(x), y))$ as $l(f(x))$ in this section.

4.1.1. Regularization in the Input Space. Based on the implication that regularizing input space smoothness benefits transferability shown in Sec. 2.2, one should directly optimize the loss surface curvature. However, it is challenging to realize it since the computationally expensive second-order derivative is involved, *i.e.*, $\nabla_x^2 \ell(f_\theta(x))$. Fortunately, deep learning and optimization theory [11] allow us to use the first-order derivative to approximate it. We thus choose two well-known first-order gradient regularizations as follows:
Input gradient regularization (*IR*): *IR* directly adds the Euclidean norm of gradient *w.r.t.* input to loss function as:

$$L_{ir} = \frac{1}{\|\mathbf{S}\|} \sum_{i=1}^{\|\mathbf{S}\|} [\ell(f(x_i)) + \lambda_{ir} \|\nabla_x \ell(f(x_i))\|],$$

where λ_{ir} controls the regularization magnitude. *IR* has been demonstrated improving the generalization and interpretability of DNNs [11, 39]. Here we show that *IR* can also improve transferability. Regularizing $\|\nabla_x \ell(f(x))\|_2$ leads to a smaller curvature $\sigma(\nabla_x^2 \ell(x))$ because the spectral norm of a matrix is upper-bounded by the Frobenius norm, *i.e.*, $\sigma(\nabla_x^2 \ell(x)) \leq \|\nabla_x^2 \ell(x)\|_F \approx \|\nabla_x \ell(f(x))^T \nabla_x \ell(f(x))\|_F \leq \|\nabla_x \ell(f(x))\|^2$. Here we approximate the second-order derivative using the first-order derivative as suggested in [21, 33]. Consequently, smaller $\sigma(\nabla_x^2 \ell(x))$ indicates better smoothness, thereby improving transferability.
Input Jacobian regularization (*JR*): *JR* regularizes gradients on the logits output of the network as:

$$L_{jr} = \frac{1}{\|\mathbf{S}\|} \sum_{i=1}^{\|\mathbf{S}\|} [\ell(f_\theta(x_i) + \lambda_{jr} \|\nabla_x f_\theta(x_i)\|_F].$$

JR has been also correlated with the generalization and robustness [21, 59]. Since *JR* has a similar form with *IR*, it is reasonable to presume that they have a similar effect. Formally, we prove that when $\|\nabla_x f_\theta(x_i)\|_F \to 0$, we have $\|\nabla_x \ell(f_\theta(x_i))\| \to 0$ using cross-entropy loss as an example (see Proposition 1). This implies that *JR* also has a positive effect on model smoothness.

4.1.2. Regularization in the Weight Space. Recently, researchers paid attention to the gradient regularization on θ, *i.e.*, the parameters (weights) of the network. A recent study [7] proved that the gradient regularizing pressure on the weight space $\|\nabla_\theta f_\theta(x)\|_F$ can transfer to the input space $\|\nabla_x f_\theta(x)\|_F$. Consequently, regularizing gradients *w.r.t.* the weight space could also implicitly promote the smoothness in the input space. We next explore two representative weight gradient regularization methods as follows:
Explicit gradient regularization (*ER*): In *ER*, the Euclidean norm of gradient *w.r.t.* θ is added to the training loss L_{er} to promote flatness as:

$$L_{er}(\theta) = L(\theta) + \frac{\lambda_{er}}{2} \|\nabla_\theta L(\theta)\|^2,$$

where L is the original objective function. *ER* has been empirically studied on improving generalization [14, 42], while we investigate it from the transferability perspective.
Sharpness-aware minimization (*SAM*): *SAM* also seeks flat solution in the weight space. Specifically, it intends

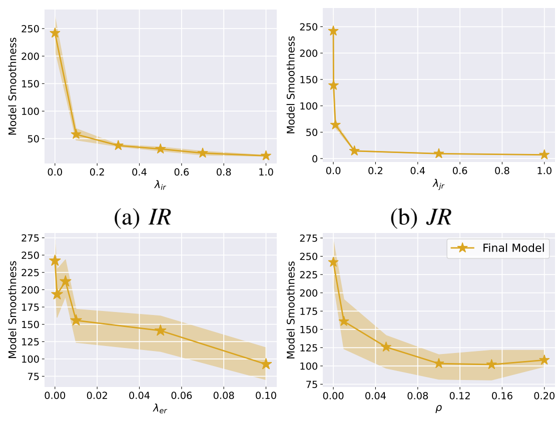

(a) *IR* (b) *JR*

(c) *ER* (d) *SAM*

Figure 9: Model smoothness of regularized models on CIFAR-10 with respective error bars at each τ. The standard accuracy of these models ranges from 90.12% to 95.38%.

to minimize the original training loss and the worst-case sharpness $L_{sam}(\theta) = L(\theta) + [\max_{\|\hat{\boldsymbol{\theta}}-\boldsymbol{\theta}\|_2 \leq \rho} L(\hat{\theta}) - L(\theta)] = \max_{\|\hat{\boldsymbol{\theta}}-\boldsymbol{\theta}\|_2 \leq \rho} L(\hat{\theta})$, where ρ denotes the radius to search for the worst neighbor $\hat{\theta}$. As the exact worst neighbor is difficult to track, *SAM* uses the gradient of ascent direction neighbor for the update after twice approximations:

$$\nabla_\theta L_{sam}(\theta) \approx \nabla_\theta L(\theta + \rho \frac{\nabla_\theta L(\theta)}{||\nabla_\theta L(\theta)||}).$$

Recent researches establish *SAM* as a special kind of gradient normalization [22, 62], where ρ represents the regularization magnitude. *SAM* has been extensively studied recently for its remarkable performance on generalization [2, 12, 51]. In this paper, for the first time, we substantiate that *SAM* also features outstanding superiority in boosting transferability.

4.2. Gradient Regularization Promotes Smoothness

We train multiple regularized models for each regularization and use coarse-grained parameter intervals [12, 39, 42] and restrict the largest regularized magnitude to avoid excessive regularization such that the accuracy of these models are above 90%. This allows for a fair comparison of each regularization method in an acceptable accuracy range. We choose 5 parameters in each interval through random grad and binary choices (See Tab. 11).

Figs. 9 and 10 depict the model smoothness. We can observe gradient regularizations generally result in smoother models (*i.e.*, smaller values) than the baseline where the regularization magnitude is 0 (*ST*), and large magnitudes correspond to better smoothness. Moreover, input gradient regularizations yield much better and stabler (smaller variance) smoothness than weight gradient regularizations, particularly on CIFAR-10. **This indicates that the transfer effect from the weight space to the input space suggested in [7] does exist, yet is somewhat marginal and cannot outperform direct regularizations in the input space.**

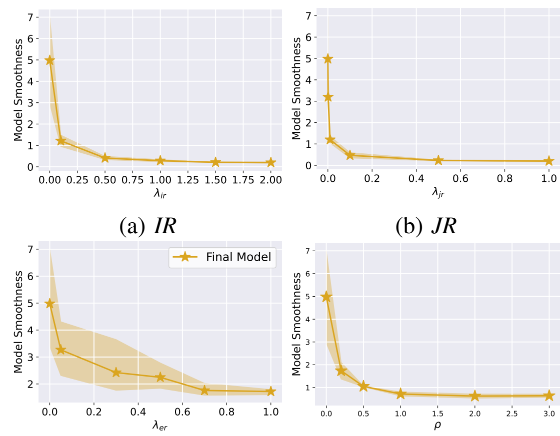

(a) *IR* (b) *JR*

(c) *ER* (d) *SAM*

Figure 10: Model smoothness of regularized models on ImageNette with respective error bars at each τ. The standard accuracy of these models ranges from 90.62% to 96.91%.

4.3. Trade-off Under Gradient Regularization

One might presume that input gradient regularization (*JR*, *IR*) should clearly outperform weight gradient regularization (*SAM*, *ER*) in terms of transferability, which agrees with the conclusion that less complexity should exhibit better transferability in Demontis *et al.* [5], given that smoothness is positively correlated to the model complexity (as analyzed in Sec. 6, **Q3**). However, our experimental results counter this:

- In Tab. 2 (CIFAR-10), the fact is that *SAM* is generally better than *IR* (11 out of 12 cases for untargeted attacks, 12 out of 12 for targeted), and generally better than *JR* (11 out of 12 cases for untargeted, 7 out of 12 for targeted).
- In Tab. 3 (ImageNette), the fact is that *SAM* is generally worse than IR (11 out of 12 cases for untargeted, 10 out of 12 for targeted), and consistently worse than *JR* (12 out of 12 cases for both targeted and untargeted).

Therefore, **these inconsistent results do not allow us to conclude that better smoothness always leads to better or worse transferability**. This finding not only weakens the conclusion in Demontis *et al.* [5], but also suggests an overall examination of these training mechanisms for superior surrogates, as they may weigh differently on similarity.

5. Boosting Transferability from Surrogates

Although we have concluded that gradient regularization can generally improve smoothness, the intangible nature of gradient similarity towards unknown target models still makes it difficult to guide us in obtaining better surrogates. We thus propose a general solution that can simultaneously improve smoothness and similarity, under a strict black-box scenario where target models are inaccessible. Our strategy involves first examining the pros and cons of various training mechanisms *w.r.t.* smoothness and similarity, and then combining their strengths to train better surrogates.

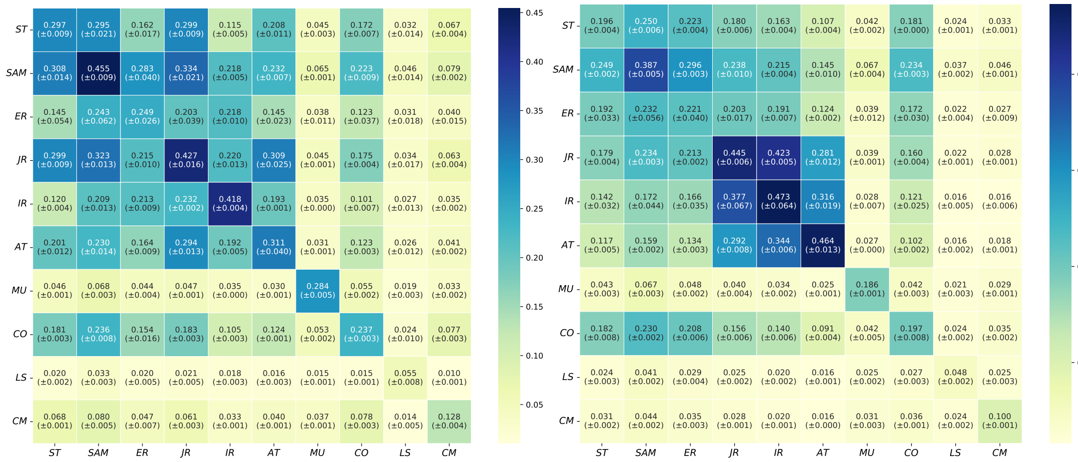

(a) ResNet18 trained over CIFAR-10

(b) ResNet50 trained over ImageNette

Figure 11: **Intra-architecture** gradient similarity between different mechanisms. Each cell reports the average result of 3 unique source-target pairs while all pair of models are trained with different random seeds, hence each matrix is asymmetric.

While gradient similarity cannot be directly measured when target models are unknown, one can assess the similarity between all the training mechanisms under the intra-architecture case instead. This helps to draw general conclusions that can be extended to the cross-architecture case as the angles between gradient directions follow the *triangle inequality*. Therefore, we measure the similarity between the surrogates we obtained thus far, reported in Fig. 11. Tab. 7 in Sec. 6, **Q2** can support the consistency posteriorly with observations in the cross-architecture case. As a result, we obtain surrogates featuring both superior smoothness and similarity on average, and extensive experiments demonstrate their superiority in transferability.

5.1. A General Route for Better Surrogates

We first elaborate on some general observations about gradient regularization mechanisms as follows:

- **Input regularizations stably yield the best smoothness.** Figs. 9 and 10 show that *IR* and *JR* yield superior smoothness and their variances are small. This does not hold for other smoothness-benefiting mechanisms like *SAM*, *ER*. Further, Fig. 11 suggests that *IR*, *JR*, and *AT* align superiorly well with each other, this could be attributed to the fact that they all have a direct penalty effect on the input space, as analyzed in Secs. 2.3 and 4.1.1.
- ***SAM* yields the best gradient alignments when input regularizations are not involved.** Fig. 11 shows that *SAM exclusively exhibits better alignment towards every mechanism* than *ST*. However, other mechanisms do not exhibit this advantage. Furthermore, if we exclude the diagonal elements, we can find *SAM* yields the best gradient similarity in each row and column except for the cases of *IR*, *JR*, and *AT*. This suggests that *SAM* has an underlying benefit on gradient similarity, which all the other mechanisms do not hold. We defer the detailed analysis on this to Sec. 6, **Q7**.
- **No single mechanism can dominate both datasets.** From Tabs. 2 and 3, we observe that *SAM* yields the best ASRs on average on CIFAR-10. However, it generally performs worse than *IR* and *JR* on ImageNette. *ER*, on the other hand, consistently performs the worst on two datasets. Apparently, there is no one mechanism that can adequately outperform the others on both datasets.

The above observations inspire us that *SAM* and input regularization are highly complementary, and a straightforward solution to reach a better trade-off between model smoothness and gradient similarity is combining *SAM* with input regularization, namely *SAM&IR* or *SAM&JR*. In other words, we believe *SAM&IR* and *SAM&JR* will bring significant improvement in transferability. To validate this hypothesis, we conduct experiments on both CIFAR-10 and ImageNette and report the results on Tabs. 2 and 3 for comparison. We can see that *SAM&JR* and *SAM&IR* generally perform the best in both datasets. Notably, we do not limit the route of constructing better surrogates to *SAM&IR* or *SAM&JR*, and there may exist other effective combinations or approaches as long as the trade-off is well reconciled.

5.2. Incorporating Surrogate-independent Methods

We show that the surrogates obtained from our methods (*e.g.*, *SAM* and *SAM&JR*) can be integrated with surrogate-independent methods to further improve transferability.

5.2.1. Incorporating AE generation strategies. Exploiting the generation process of AEs is a popular approach to improve transferability. The most representative methods include *momentum iterative* (MI) [8] and *diversity iterative* (DI) [56], and DI is frequently combined with MI and serves as a stronger baseline—*diversity iterative with momentum* (DIM). Generally, these designs are interpreted as constructing adversarial examples that are less likely to fall into a poor local optimum of the given surrogate. Thus they adjust the update direction with momentum to escape

TABLE 4: Untargeted and targeted transfer ASRs (in %) when incorporating AE generation strategies under the different L_∞ budgets on CIFAR-10. Corresponding results are different from those of Tab. 2 due to different randomizations.

	Untargeted								Targeted							
	4/255				8/255				4/255				8/255			
	Res-50	VGG16	Inc-V3	Dense-121	Res-50	VGG16	Inc-V3	Dense-121	Res-50	VGG16	Inc-V3	Dense-121	Res-50	VGG16	Inc-V3	Dense-121
ST	55.0±2.4	43.3±2.1	54.9±2.5	71.7±1.2	79.6±2.6	71.3±3.2	80.2±3.8	93.1±1.3	19.0±1.2	13.2±1.0	21.1±1.5	36.4±1.8	41.1±4.7	34.3±3.7	45.8±4.2	70.8±4.6
SAM	76.8±4.7	65.0±5.3	74.9±0.6	87.4±1.2	97.5±1.2	94.3±2.2	97.0±0.2	99.5±0.1	37.1±6.4	27.2±5.0	38.5±2.0	55.8±3.7	77.2±9.2	68.3±8.4	78.4±2.7	93.4±0.9
SAM&JR	**81.2**±0.7	**70.2**±0.7	**79.4**±0.6	**91.3**±0.1	**98.7**±0.3	**96.6**±0.1	**98.3**±0.0	**99.8**±0.0	**43.6**±2.1	**32.9**±1.2	**45.3**±2.1	**64.5**±0.9	**85.4**±1.4	**77.2**±9.2	**86.8**±1.9	**97.2**±0.3
ST+MI	58.4±2.6	45.0±2.9	58.7±4.0	76.7±2.3	82.9±3.1	75.6±4.1	83.5±3.6	94.6±1.2	22.4±1.8	15.4±1.9	25.6±2.8	46.0±3.9	44.8±4.1	40.2±5.9	50.4±6.3	76.1±4.5
SAM+MI	82.3±3.9	69.6±5.3	80.5±0.1	91.7±1.5	98.1±0.9	95.5±1.9	97.8±0.1	99.7±0.1	46.7±7.0	33.2±5.7	49.0±1.1	69.6±3.8	84.0±6.9	76.9±5.8	84.8±1.2	96.4±0.9
SAM&JR+MI	**85.0**±0.4	**73.8**±0.5	**83.3**±0.5	**93.6**±0.1	**98.9**±0.2	**97.2**±0.2	**98.7**±0.1	**99.8**±0.1	**52.4**±2.0	**38.4**±1.5	**54.0**±1.7	**74.5**±0.4	**89.6**±1.6	**82.9**±1.5	**90.6**±2.1	**98.3**±0.3
ST+DIM	70.2±3.8	59.2±2.7	69.2±3.5	83.6±3.1	91.9±2.2	88.3±2.8	91.7±2.2	97.2±1.3	33.6±4.8	25.7±3.2	36.6±4.2	54.9±6.3	65.4±6.3	62.0±6.2	69.9±5.3	87.5±5.3
SAM+DIM	**84.4**±2.6	74.7±2.7	**82.2**±1.8	91.8±2.2	98.9±0.4	97.7±0.7	**99.1**±0.8	99.7±0.2	50.4±4.6	38.9±3.2	51.3±4.2	67.8±5.8	89.3±3.5	84.2±2.2	89.6±3.0	96.8±1.9
SAM&JR+DIM	83.6±1.6	**74.8**±1.0	81.8±1.4	**92.1**±0.6	**99.2**±0.2	**98.2**±0.3	99.0±0.1	**99.8**±0.1	**51.6**±3.9	**40.7**±2.4	**52.7**±2.9	**70.2**±2.0	**91.5**±2.9	**86.9**±2.8	**91.8**±2.6	**98.1**±0.8

TABLE 5: Untargeted and targeted transfer ASRs (in %) of AEs crafted against single and LGV ensemble surrogates under the different L_∞ budgets on CIFAR-10. Initial surrogates without fine-tuning are used for baselines and compared with LGV ensembles. We highlight the best ASRs in bold and those lower than baselines in red for each comparison.

	Untargeted								Targeted							
	4/255				8/255				4/255				8/255			
	Res-50	VGG16	Inc-V3	Dense-121	Res-50	VGG16	Inc-V3	Dense-121	Res-50	VGG16	Inc-V3	Dense-121	Res-50	VGG16	Inc-V3	Dense-121
ST	55.0±2.4	43.3±2.1	54.9±2.5	71.7±1.2	79.6±2.6	71.3±3.2	80.2±3.8	93.1±1.3	19.0±1.2	13.2±1.0	21.1±1.5	36.4±1.8	41.1±4.7	34.3±3.7	45.8±4.2	70.8±4.6
ST+LGV$_{\text{SGD}}$	70.7±2.2	57.1±1.1	70.1±0.9	87.1±0.6	94.0±2.0	89.1±2.5	94.3±1.8	99.3±0.2	29.3±2.0	20.4±1.3	32.8±2.1	53.4±2.1	65.6±4.2	56.8±3.2	71.3±2.5	92.0±1.2
ST+LGV$_{SAM}$	79.5±0.8	66.8±1.1	79.8±1.0	92.3±0.2	98.6±0.2	96.0±0.5	98.7±0.2	**99.9**±0.0	39.4±1.0	27.7±0.5	44.4±1.7	65.7±0.9	82.5±1.7	74.2±1.0	87.4±0.8	97.8±0.2
ST+LGV$_{SAM\&JR}$	**82.0**±1.5	**69.5**±1.7	**81.3**±1.3	**93.4**±0.3	**99.1**±0.3	**97.1**±0.7	**99.0**±0.2	**99.9**±0.0	**42.9**±2.6	**30.3**±1.5	**46.7**±1.4	**68.1**±1.0	**87.1**±3.5	**79.1**±3.4	**90.2**±1.7	**98.5**±0.3
SAM	76.8±4.7	65.0±5.3	74.9±0.6	87.4±1.2	97.5±1.2	94.3±2.2	97.0±0.2	99.5±0.1	37.1±6.4	27.2±5.0	38.5±2.0	55.8±3.7	77.2±9.2	68.3±8.4	78.4±2.7	93.4±0.9
SAM+LGV$_{\text{SGD}}$	70.8±6.1	57.2±6.5	69.2±0.7	84.2±0.7	93.1±3.9	87.6±5.3	93.2±1.4	98.6±0.3	26.7±1.9	18.7±0.1	31.5±2.2	51.3±2.6	63.6±14.1	53.6±11.8	66.4±5.4	87.6±2.2
SAM+LGV$_{SAM}$	81.5±4.0	69.5±4.8	79.8±1.3	91.6±1.3	98.9±0.7	96.9±1.3	98.7±0.1	**99.9**±0.0	42.1±7.3	30.5±5.5	44.3±1.6	63.4±1.9	86.2±6.7	78.4±6.6	87.9±1.1	97.5±0.4
SAM+LGV$_{SAM\&JR}$	**82.7**±4.2	**71.2**±5.1	**80.9**±0.6	**92.1**±1.2	**99.1**±0.6	**97.4**±1.3	**99.0**±0.3	**99.9**±0.0	**44.7**±7.7	**32.6**±5.9	**46.6**±0.6	**65.6**±1.7	**87.6**±6.9	**79.8**±7.1	**89.1**±2.0	**97.9**±0.5
SAM&JR	81.2±0.7	70.2±0.7	79.4±0.6	91.3±0.1	98.7±0.3	96.6±0.1	98.3±0.0	99.8±0.0	43.6±2.1	32.9±1.2	45.3±2.1	64.5±0.9	85.4±1.4	77.2±2.1	86.8±1.9	97.2±0.3
SAM&JR+LGV$_{\text{SGD}}$	73.8±1.8	61.1±1.6	73.1±1.8	88.3±0.5	95.8±1.1	90.9±1.9	95.6±1.1	99.4±0.1	35.6±2.9	25.1±2.4	39.0±2.7	60.2±1.7	70.5±5.0	61.1±5.9	74.5±5.7	93.6±1.5
SAM&JR+LGV$_{SAM}$	82.5±0.7	71.2±1.0	81.0±0.4	93.0±0.2	99.1±0.1	97.4±0.2	98.9±0.1	**99.9**±0.1	44.0±1.5	32.2±1.1	46.8±1.4	67.6±0.8	87.6±1.2	80.2±1.7	89.7±1.2	98.4±0.1
SAM&JR+LGV$_{SAM\&JR}$	**83.8**±0.8	**72.9**±1.2	**82.5**±0.9	**93.7**±0.1	**99.3**±0.1	**97.8**±0.3	**99.3**±0.1	**99.9**±0.0	**46.9**±1.4	**34.8**±1.2	**49.5**±1.0	**70.0**±0.5	**90.0**±0.9	**83.2**±0.7	**91.8**±0.7	**98.8**±0.1

it or apply multiple transformations on inputs to mimic an averagely flat landscape. We conduct experiments to verify that obtaining a better surrogate, which features less and wider local optima (analyzed in Sec. 6, **Q3**) and general adversarial direction, can further enhance these designs by promoting a larger lower bound.

In Tab. 4, the transfer ASRs under different generation strategies (PGD, MI, and DIM) show that using better surrogates can always significantly boost transferability. This suggests that the optima found in *ST* are inherently poorer than those in *SAM* and *SAM&JR*. Besides, without MI or DIM, *SAM&JR* using standard PGD alone already outperforms *ST*+MI and *ST*+DMI, implying that the lower bound of transferability in a better surrogate is sufficiently high, and even surpasses the upper bound in poor models.

5.2.2. Incorporating ensemble strategies. Using multiple surrogates is widely believed to update adversarial examples in a more general direction that benefits transferability. Recently, [17] proposed constructing the ensemble from a *large geometric vicinity* (LGV), *i.e.*, first fine-tuning a normally trained model with a high constant learning rate to obtain a set of intermediate models that belongs to a large vicinity, then optimizing AEs iteratively against all these models. We conduct experiments to verify whether *SAM* and *SAM&JR* can further enhance this ensemble and analyze how their intrinsic mechanisms correlate with LGV. Specifically, we fine-tune models well-trained with SGD[3], *SAM*, and *SAM&JR* on CIFAR-10 using SGD, *SAM*, and *SAM&JR* with a constant learning rate of 0.05.

3. We refer SGD here to training models without any augmentation or regularization mechanisms, not merely the particular optimizer itself.

In Tab. 5, the transfer results show that LGV with *SAM*, *SAM&JR* can always yield superior ASRs than standard SGD, indicating that the underlying property of *SAM* and *JR* allows them to find solutions that benefit transferability. More intriguingly, fine-tuning models obtained by *SAM* and *SAM&JR* with SGD always brings non-negligible negative impacts on transferability. These suggest solutions well-trained with *SAM* and *SAM&JR* lie in the *basin of attractions* featuring better transferability, and a relatively high constant learning rate with SGD will arbitrarily minimize the training loss while leaving the basin of attractions. Note that a relatively high constant learning rate is necessary for a large vicinity [17], thus we can infer that a large vicinity may not be a determining factor for transferability since a single surrogate can outperform an ensemble of poor surrogates (see *SAM&JR* and *ST*+LGV$_{\text{SGD}}$). Instead, a dense subspace whose geometry is intrinsically connected to transferability is more desirable.

5.2.3. Incorporating other strategies. We take AE generation and ensemble strategies, which are the most well-explored methods, to exemplify the universality of better surrogates. We are aware of other factors that could also contribute to transferability, such as loss object modification [63], architecture selection [53], l_2-norm consideration [32], unrestricted generation [19], patch-based AEs [20]. We leave it to our future work to investigate whether they can be mildly integrated with our design.

6. Analyses and Discussions

Q1: Does the trade-off between smoothness and similarity really "significantly indicate" transferability *w.r.t.*

TABLE 6: The Pearson correlation coefficients (r) between ASR and accuracy (Acc), fooling probability (FP), model smoothness (MS), and gradient similarity (GS). For the coefficient of determination (R^2) in OLS, R_1^2 depicts the joint effect of MS and GS on ASR and R_2^2 depicts the joint effect of these 4 factors.

CIFAR-10	ResNet50			VGG16			InceptionV3			DenseNet121		
	$\frac{4}{255}$	$\frac{8}{255}$	$\frac{16}{255}$	$\frac{4}{255}$	$\frac{8}{255}$	$\frac{16}{255}$	$\frac{4}{255}$	$\frac{8}{255}$	$\frac{16}{255}$	$\frac{4}{255}$	$\frac{8}{255}$	$\frac{16}{255}$
$r(Acc, ASR)$	0.121	-0.049	-0.255	0.032	-0.095	-0.259	0.211	0.028	-0.187	0.286	0.130	-0.107
$r(FP, ASR)$	0.118	0.106	0.055	0.197	0.164	0.098	0.105	0.091	0.040	0.051	0.008	-0.033
$r(MS, ASR)$	0.540	0.662	0.753	0.614	0.700	0.774	0.478	0.630	0.732	0.418	0.581	0.701
$r(GS, ASR)$	0.912	0.837	0.759	0.924	0.878	0.816	0.864	0.743	0.653	0.875	0.710	0.585
R_1^2	0.909	0.885	0.879	0.917	0.906	0.893	0.870	0.827	0.838	0.880	0.773	0.765
R_2^2	0.943	0.892	0.894	0.931	0.907	0.913	0.911	0.843	0.852	0.926	0.823	0.799
ImageNette	VGG16			DenseNet121			MobileNetV2			Xception		
	$\frac{4}{255}$	$\frac{8}{255}$	$\frac{16}{255}$	$\frac{4}{255}$	$\frac{8}{255}$	$\frac{16}{255}$	$\frac{4}{255}$	$\frac{8}{255}$	$\frac{16}{255}$	$\frac{4}{255}$	$\frac{8}{255}$	$\frac{16}{255}$
$r(Acc, ASR)$	0.218	0.128	-0.047	0.133	0.023	-0.165	0.093	-0.014	-0.196	0.072	-0.028	-0.177
$r(FP, ASR)$	0.121	0.120	-0.055	0.146	0.117	-0.081	-0.034	0.003	-0.151	0.062	-0.012	-0.156
$r(MS, ASR)$	0.410	0.472	0.516	0.458	0.503	0.492	0.495	0.576	0.625	0.499	0.571	0.624
$r(GS, ASR)$	0.864	0.829	0.764	0.859	0.855	0.853	0.789	0.766	0.780	0.753	0.722	0.721
R_1^2	0.854	0.841	0.780	0.821	0.843	0.832	0.715	0.742	0.804	0.688	0.704	0.752
R_2^2	0.871	0.847	0.798	0.854	0.850	0.867	0.750	0.752	0.833	0.712	0.707	0.781

surrogates? Our theoretical analysis and experimental validation have demonstrated the significant role of smoothness and similarity in regulating transferability among surrogate-side factors. To investigate whether their impact on transferability is significant, we calculate the respective Pearson correlation coefficients between the surrogate-related factors and ASR and run *ordinary least squares* (OLS) regressions to measure their joint effect on ASR. Tab. 6 reports the results under each fixed target model and adversarial budget, which indicates that both smoothness and similarity are highly correlated to ASR, with a clear superiority over other factors. Besides, the joint effect of smoothness and similarity (R_1^2) is significant in each case and very close to that of the 4 factors combined (R_2^2). Further, it does not exhibit a strong correlation with ϵ under each target model, indicating the joint effect is indeed strong and robust.

Interestingly, we can observe that as ϵ increases, the relevance *w.r.t.* smoothness alone increases, and the relevance *w.r.t.* similarity alone decreases. This agrees with the intuition: smoothness depicts the gradient invariance around the origin, while similarity captures the alignment of two gradients in different directions. As ϵ approaches 0, smoothness becomes less important as the gradient may not vary too much in a small region, and the legitimate direction becomes more crucial since there is limited scope for success. As ϵ gets bigger, the alignment at the origin requires better smoothness to be further propagated into a bigger region. These suggest an adaptive similarity-smoothness trade-off surrogate could be preferable given different ϵ.

Q2: What if the target model is not trained on $\mathcal{D}$? So far, we presume the target models are trained within the normal data distribution $\mathcal{D}$ to lay out our analysis and conclusions, which is also set by default in Demontis *et al*. [5]. To verify the generality of the obtained conclusion, we deliver the results here when the data distribution restrictions of target model $\mathcal{G}$ is relaxed. First, we generalize Hypothesis 1 as:

Hypothesis 2 (**$\mathcal{D}$-surrogate aligns general target models better than $\mathcal{D}'$-surrogate**). *Suppose surrogates $\mathcal{F}_{\mathcal{D}}$ and $\mathcal{F}_{\mathcal{D}'}$ are trained on $\mathcal{D}$ and $\mathcal{D}'$ respectively. Denote the data distribution of target model $\mathcal{G}_{\mathcal{D}_t}$ as $\mathcal{D}_t \in \mathcal{P}_{\mathcal{X}\times\mathcal{Y}}$. They share a joint training loss ℓ. Then $\mathbb{E}_{\mathcal{D}_t\sim\mathcal{P}_{\mathcal{X}\times\mathcal{Y}}}[\tilde{\mathcal{S}}_{\mathcal{D}}\left(\ell_{\mathcal{F}_{\mathcal{D}'}}, \ell_{\mathcal{G}_{\mathcal{D}_t}}\right) - \tilde{\mathcal{S}}\left(\ell_{\mathcal{F}_{\mathcal{D}}}, \ell_{\mathcal{G}_{\mathcal{D}_t}}\right)] < 0$ generally holds.*

This hypothesis considers a more practical case that the adversary has no knowledge of $\mathcal{D}_t$, and tries to attack $\mathcal{G}_{\mathcal{D}_t}$ with AEs constructed on normal samples $(x, y) \in \mathcal{D}$. The adversary hopes its surrogate aligns well with any $\mathcal{G}_{\mathcal{D}_t}$ regardless of what $\mathcal{D}_t$ is. We show that $\mathcal{D}$-surrogate $\mathcal{F}_{\mathcal{D}}$ is still generally better than $\mathcal{D}'$-surrogate $\mathcal{F}'_{\mathcal{D}}$ based on the expectation over various $\mathcal{D}_t$.

TABLE 7: **Cross-architecture** gradient similarity between surrogate-target pairs (ResNet18-VGG16) on CIFAR-10. The first row reports the results of *ST* surrogate, below which report the difference to *ST*. The last column rates the score of the surrogates based on the general alignment toward multiple targets. (Accumulate +1 for positive, -1 for negative values.)

Surrogate $\mathcal{F}$ \ Target $\mathcal{G}_{\mathcal{D}_t}$		*ST*	*CO*	*CM*	*MU*	*LS*	*AT*	Increment Score
$\mathcal{D}$	*ST*	0.141	0.135	0.056	0.038	0.014	0.131	0
$\mathcal{D}'$	*CO*	-0.038	+0.005	-0.001	+0.004	-0.001	-0.041	-2
	CM	-0.105	-0.084	**+0.008**	-0.021	-0.006	-0.098	-4
	MU	-0.106	-0.092	-0.030	**+0.122**	-0.003	-0.102	-4
	LS	-0.094	-0.098	-0.033	-0.013	+0.008	-0.090	-4
	AT	-0.002	-0.005	-0.013	+0.001	+0.001	+0.047	0
$\mathcal{D}$	*IR*	-0.002	-0.014	-0.020	+0.008	+0.007	+0.043	0
	JR	+0.044	+0.028	+0.004	+0.012	+0.004	+0.072	**+6**
	ER	+0.012	+0.006	-0.013	+0.011	+0.005	+0.031	+4
	SAM	+0.055	+0.057	+0.007	+0.029	+0.006	+0.058	**+6**
	SAM&IR	+0.012	+0.001	-0.021	+0.016	**+0.010**	+0.065	+4
	SAM&JR	**+0.078**	**+0.072**	**+0.008**	+0.035	**+0.010**	**+0.093**	**+6**

Tab. 7 reports the general surrogate-target gradient similarities. It is obvious that $\mathcal{D}'$ surrogates (above *AT*) generally worsen the gradient alignments as their increment scores are all negative, except for *AT* with a small budget $\epsilon = 0.01$. Conversely, the scores of $\mathcal{D}$ surrogates (below *AT*) are all non-negative and most of them improve the general alignment. Note that when $\mathcal{D}'$ happens to be $\mathcal{D}_t$, the gradient similarity between $\mathcal{F}'_{\mathcal{D}}$ and $\mathcal{G}_{\mathcal{D}_t}$ is high, especially for *CM* and *MU*. However, these surrogates lower the similarity towards all other targets. In general, they are not good surrogates since $\mathcal{D}_t$ is unknown to the adversary.

The same observations apply to the transfer ASRs. Tab. 8 reports the transfer ASRs against various $\mathcal{G}_{\mathcal{D}_t}$ that are not trained on $\mathcal{D}$. Even when surrogates have the same training mechanisms as the corresponding target models, the best surrogate is still either *SAM&IR* or *SAM&JR*, regardless of what $\mathcal{D}_t$ is. This finding is in line with the results in Tab. 2.

Q3: What is the relationship between model smoothness and model complexity? Model complexity has been investigated in Demontis *et al*. [5] to figure out whether it correlates with transferability, which is defined as the variability of the loss landscape, deriving from the number of local optima of the surrogates. Here we correlate the number of local optima with model smoothness. It is obvious that a high-complexity model featuring multiple local optima will cause a larger variance to the loss landscape of AE optimization. Formally, for a feature x, the fewer optima in its ϵ-neighbor,

TABLE 8: Transfer ASRs of AEs crafted from various ResNet18 surrogates against VGG16 target models trained with *AT* and augmentations on CIFAR-10. ★ denotes that surrogates have the same training methods as the corresponding target models. 'T' represents 'Targeted' attack and 'U' represents 'Untargeted' attack.

	AT, $\epsilon = 0.01$		*AT*, $\epsilon = 0.05$		*CM*		*CO*		*LS*		*MU*	
	T	U	T	U	T	U	T	U	T	U	T	U
ST	20.18	51.33	4.83	22.49	42.42	79.49	38.80	76.33	34.62	72.34	37.46	69.25
★	43.01	76.96	35.54	69.56	14.20	54.57	32.91	79.11	11.90	46.66	15.81	54.43
IR	60.08	91.23	31.84	73.98	59.80	91.82	60.78	92.14	63.20	93.52	60.79	90.06
JR	57.24	83.54	14.57	41.77	73.44	92.47	74.77	93.03	72.27	92.30	68.34	86.90
ER	32.61	77.14	9.55	40.41	41.94	86.92	43.04	87.39	44.51	87.77	42.12	82.66
SAM	40.35	79.31	8.41	35.05	75.34	96.59	67.72	94.84	62.68	93.57	65.37	90.43
SAM&IR	**71.88**	**94.01**	**48.38**	**80.88**	70.81	93.75	73.05	94.31	74.02	95.47	70.81	92.68
SAM&JR	58.81	89.23	15.11	47.11	**83.56**	**97.57**	**80.19**	**97.02**	**77.95**	**96.92**	**75.06**	**94.49**

the smaller the variance would be. Thus, supposing the loss function used to optimize adversarial points is continuously differentiable, by promoting the smoothness, we can expect fewer optima in the finite ϵ-neighbor space since all the local optima are wider. Consequently, model smoothness negatively correlates with model complexity, *i.e.*, a smoother model indicates lower complexity.

Q4: Does a smaller model generalization gap imply higher adversarial transferability? It is natural to raise this question as the idea of adversarial transferability in a way resembles the concept of model generalization. The former captures the effectiveness of AEs against unseen models, while the latter evaluates the model's ability to adapt properly to previously unseen data. A concurrent work [50] attempts to show the positive relationship between model generalization and adversarial transferability, by applying a spectral normalization method constraining the L_2-operator norm of the surrogate's weight matrix to empirically demonstrate the increase of both transferability and generalization.

Nevertheless, we emphasize that such alignment between generalization and transferability cannot be over-generalized. It is easy to find some cases that boost generalization yet degrades transferability (*e.g.*, through damaging similarity). For example, the results in Tabs 2, 3, 10, and 13 have shown augmentations that boost generalization could impair transferability. More typically, the strong data augmentations that yield the smallest generalization gaps (*MU*, *CM* in Tab. 12) perform the worst in transfer attacks. In fact, the product of spectral norm of model's layer-wise weight matrices is a loose upper bound of $\|\nabla_x f_\theta(x)\|_2$ [40, 59]. When $\|\nabla_x f_\theta(x)\|_2 \rightarrow 0$, we have $\|\nabla_x f_\theta(x)\|_F \rightarrow 0$. Utilizing Proposition 1, we also have $\|\nabla_x \ell(f_\theta(x), y)\| \rightarrow 0$. This suggests that spectral normalization actually benefits transferability by promoting smoothness.

Q5: What is restraining the adversarial transferability of ViT? Recently, ViT [10] receives notable attention for its outstanding performance on various tasks. Meanwhile, some works [31, 41] have demonstrated that ViT models exhibit lower adversarial transferability than CNNs when used as surrogates, and a recent work [36] argues that this is because the current attacks are not strong enough to fully exploit the transferability potential of ViT. Complementarily, we provide a different viewpoint that *the transferability of ViT may have been restrained by its own training paradigm*. ViT is known to have poor trainability [2, 3], and thus generally requires large-scale pre-training and fine-tuning with strong data augmentations. This training paradigm is used by default since its appearance. However, as we discussed in this paper, changing the data distribution could have negative impacts on similarity. Using data augmentation is plausible for accuracy performance, yet not ideal for transfer attacks.

TABLE 9: Untargeted transfer ASRs (in %) of AEs crafted against ViT ImageNet surrogates on target models

Source	Acc	Normally Trained				Adversarially Trained	
		Res101	Dense121	VGG16	IncV3	IncV3_{AT}	IncResV3_{AT}
ViT-B/16	**84.5**	23.8	37.6	50.0	45.9	48.6	27.6
ViT-B/16-*SAM*	80.2	**48.4**	**69.9**	**75.2**	**70.2**	**59.5**	**40.5**
ViT-B/32	**80.7**	19.6	35.7	50.0	49.1	51.9	29.7
ViT-B/32-*SAM*	73.7	**34.0**	**55.8**	**68.9**	**64.3**	**63.1**	**43.9**
ViT-B/16+DIM	**84.5**	60.7	75.3	79.9	80.0	61.4	43.8
ViT-B/16-*SAM*+DIM	80.2	**81.6**	**95.6**	**93.9**	**94.6**	**82.4**	**79.9**
ViT-B/32+DIM	**80.7**	48.4	66.4	75.2	81.6	68.6	54.4
ViT-B/32-*SAM*+DIM	73.7	**48.9**	**78.1**	**78.4**	**82.5**	**79.3**	**72.3**

To validate this standpoint, we show that with a different training method such as *SAM*, the transferability of ViT can be significantly improved. Our experiments are conducted on well-trained ImageNet classifiers, all publicly available from PyTorch image model library timm [52]. We consider standard ViT surrogates ViT-B/16 and ViT-B/32, which are both first pre-trained on a large-scale dataset and then fine-tuned on ImageNet using a combination of *MU* and RandAugment [4]. In contrast, their *SAM* versions ViT-B/16-*SAM* and ViT-B/32-*SAM* are merely trained from scratch. We use both normally and adversarially trained CNN classifiers as target models. We craft AEs on these 4 surrogates using both standard PGD and DIM under $\epsilon = 16/255$ on the ImageNet-compatible dataset as in [38]. The accuracy of these surrogates (referring to [52]) and ASRs are reported in Tab. 9. The results indicate that standard ViT models have much weaker transferability than their *SAM* versions, despite the fact that they have higher accuracy.

Q6: Will the transferability benefit of better surrogate in "lab" generalize to "real-world" environment? Recently, Mao *et al*. [32] suggests that many conclusions about adversarial transferability done in the simplistic controlled "lab" environments may not hold in the real world. We thus conduct experiments to verify the generality of our conclusions using AEs crafted against our ImageNette surrogates.

Specifically, aligning with Mao *et al*. [32], we conduct transfer attacks on three commercial MLaaS platforms—AWS Rekognition, Alibaba Cloud, and Baidu Cloud, using their code, and report the results in Tab. 10. The results are generally consistent with that in Tab. 3. Particularly, we highlight here that our experimental results on MLaaS platforms **contradict** the observation in Mao *et al*. [32] that "adversarial training and data augmentation do not show strong correlations to the transfer attack". Tab. 10 indicates that strong data augmentations like *CM* and *MU* generally exhibit lower ASRs than *ST* for both targeted and untargeted attacks. In addition, we can observe that "little robustness" (see *AT*, $\epsilon = 1$) improves transferability while large adversarial magnitude (see *AT*, $\epsilon = 5$) degrades it.

TABLE 10: Transfer ASRs (in %) under the different L_∞ budgets on 3 MLaaS platforms using AEs reported in Tab. 3

Model	Untargeted						Targeted					
	AWS		Baidu		Aliyun		AWS		Baidu		Aliyun	
	$\frac{8}{255}$	$\frac{16}{255}$	$\frac{8}{255}$	$\frac{16}{255}$	$\frac{8}{255}$	$\frac{16}{255}$	$\frac{8}{255}$	$\frac{16}{255}$	$\frac{8}{255}$	$\frac{16}{255}$	$\frac{8}{255}$	$\frac{16}{255}$
ST	9.4	13.4	30.0	53.8	18.6	52.2	23.0	23.8	11.6	16.6	2.6	6.4
MU	8.6	10.8	20.4	39.6	12.4	33.8	20.4	23.8	9.6	15.0	1.4	2.8
CM	8.0	10.8	19.4	35.0	12.4	29.2	22.2	23.0	10.0	11.2	1.2	3.0
CO	9.6	13.0	27.2	48.4	18.6	51.8	23.2	26.4	14.0	16.8	2.0	6.8
LS	9.6	12.0	23.4	43.0	12.2	33.6	22.2	23.0	12.6	14.4	1.4	2.0
AT, $\epsilon = 1$	9.6	24.0	38.2	60.4	35.0	82.6	24.8	33.2	14.8	27.6	3.6	13.8
AT, $\epsilon = 5$	7.8	16.0	22.2	53.4	15.6	60.0	22.0	27.6	11.0	17.0	1.2	5.0
IR	10.4	23.6	45.8	60.0	48.8	86.0	25.0	34.4	17.2	26.4	8.0	15.4
JR	9.8	22.6	46.4	60.6	48.2	79.6	26.8	32.0	17.2	25.0	7.8	12.4
ER	9.8	13.4	28.2	56.2	24.0	56.6	23.8	26.4	14.2	20.0	3.2	8.0
SAM	10.2	16.4	37.2	59.2	36.2	68.2	23.4	30.0	13.8	19.2	4.6	9.8
SAM&IR	11.0	28.4	54.2	63.8	55.8	93.4	29.2	36.2	16.8	28.0	9.8	18.0
SAM&JR	11.4	16.2	45.8	61.2	48.0	79.0	25.4	33.2	18.8	21.8	8.2	11.8

Q7: How does *SAM* yield superior alignment towards every training solution? Given its superior performance on transferability and gradient alignment, it is natural to wonder why *SAM* exhibits this property. Recent works [16, 25] empirically demonstrate that attacking an ensemble of models in the distribution obtained via *Bayesian* learning substantially improves the transferability. Another concurrent work [34] theoretically establishes *SAM* as an optimal relaxation of Bayes object. Consequently, this suggests that the transferability benefit of *SAM* may be attributed to the fact it optimizes a single model that represents an ensemble (expectation) of models, *i.e.*, attacking a *SAM* solution is somewhat equivalent to attacking an ensemble of solutions. We conjecture that the strong input gradient alignment towards every training solution may reflect this "expectation" effect of *SAM* (Bayes). Notably, our interpretation here is merely intuitive and speculative, and *SAM* remains poorly understood to date, especially with its generalization benefit. We believe that uncovering the exact reason is far beyond the scope of our study, while our experimental observations provide valuable insights and may contribute to a better understanding of *SAM* for future study.

7. Related Work

Our aim is to provide a comprehensive overview of adversarial transferability from the surrogate training perspective. We examine how model smoothness and gradient similarity are affected under various training mechanisms.

Intriguingly, we notice that some concurrent works also adopt similar design philosophies from other perspectives of transferability. Wu *et al.* [54] and Ge *et al.* [13] both suggest a regularization term that encourages small loss gradient norms in the input space during AE generation. On the other hand, Chen *et al.* [1] study transferability from the model ensemble perspective and propose a common weakness attack, which aims to converge AEs to points close to the flat local optimum of each model. These works also demonstrate the effectiveness of optimizing smoothness and similarity for improving transferability in AEs generation.

Other approaches that study from the surrogate perspective transform the model at test time (*i.e.*, after training, when performing the attack). Ghost network [26] attacks a set of ghost networks generated by densely applying dropout at intermediate features. SGM [53] incorporates more gradients from the skip connections of ResNet to generate AEs, while LinBP [18] and BPA [49] both restore the truncated gradient from non-linear layers.

Our work complements them all since we view transferability as an inherent property of the surrogate model itself and propose methods to construct surrogate models specialized for transfer attacks at the training time. We leave the exploration of a unified framework that can reason transferability from all perspectives for future work.

8. Conclusion

In this paper, we have conducted a comprehensive analysis of the transferability of adversarial examples from the surrogate perspective. To the best of our knowledge, this is the first in-depth study on obtaining better surrogates for transfer attacks. We have proposed and examined two working hypotheses. The first one is that the trade-off between model smoothness and gradient similarity significantly indicates adversarial transferability from the surrogate model's perspective. The other one is that the data distribution shift will impair gradient similarity, thereby producing worse surrogates on average. As a result, the practical guide for more effective transfer attacks is to handle these model smoothness and similarity well simultaneously, validated by the superiority of our proposed methods, *i.e.*, the combination of input gradient regularization (*JR* and *IR*) and sharpness-aware minimization (*SAM*). On the other front, our study also exemplifies the conflicting aspects of current research and further provides plausible explanations for some intriguing puzzles while revealing other unsolved issues in the study of adversarial transferability.

Acknowledgements

We thank the anonymous reviewers and the shepherd for their valuable feedback. This work is supported by the National Natural Science Foundation of China (Grant No.U20A20177) and Hubei Province Key R&D Technology Special Innovation Project (Grant No.2021BAA032). Shengshan Hu is the corresponding author. We also would like to acknowledge that an extended version of this paper is available at https://arxiv.org/abs/2307.07873.

References

[1] H. Chen, Y. Zhang, Y. Dong, and J. Zhu. Rethinking Model Ensemble in Transfer-based Adversarial Attacks. *arXiv preprint arXiv:2303.09105*, 2023.

[2] X. Chen, C.-J. Hsieh, and B. Gong. When Vision Transformers Outperform ResNets without Pre-training or Strong Data Augmentations. In *Proceedings of the 10th International Conference on Learning Representations (ICLR'22)*, 2022.

[3] X. Chen, S. Xie, and K. He. An Empirical Study of Training Self-Supervised Vision Transformers. In *Proceedings of IEEE/CVF International Conference on Computer Vision (ICCV'21)*, pages 9640–9649, 2021.

[4] E. D. Cubuk, B. Zoph, J. Shlens, and Q. V. Le. Randaugment: Practical Automated Data Augmentation With a Reduced Search Space. In *Proceedings of the IEEE/CVF Conference on Computer Vision and Pattern Recognition Workshops (CVPRW'20)*, pages 702–703, 2020.

[5] A. Demontis, M. Melis, M. Pintor, M. Jagielski, B. Biggio, A. Oprea, C. Nita-Rotaru, and F. Roli. Why Do Adversarial Attacks Transfer? Explaining Transferability of Evasion and Poisoning Attacks. In

Proceedings of the 28th USENIX Security Symposium (Security'19), 2019.

[6] T. DeVries and G. W. Taylor. Improved Regularization of Convolutional Neural Networks with Cutout. *arXiv preprint arXiv:1708.04552*, 2017.

[7] B. Dherin, M. Munn, M. Rosca, and D. Barrett. Why Neural Networks Find Simple Solutions: the Many Regularizers of Geometric Complexity. In *Proceedings of the 36th Annual Conference on Neural Information Processing Systems (NeurIPS'22)*, pages 2333–2349, 2022.

[8] Y. Dong, F. Liao, T. Pang, H. Su, J. Zhu, X. Hu, and J. Li. Boosting Adversarial Attacks with Momentum. In *Proceedings of the 2018 IEEE Conference on Computer Vision and Pattern Recognition (CVPR'18)*, pages 9185–9193, 2018.

[9] Y. Dong, T. Pang, H. Su, and J. Zhu. Evading Defenses to Transferable Adversarial Examples by Translation-Invariant Attacks. In *Proceedings of the 2019 IEEE/CVF Conference on Computer Vision and Pattern Recognition (CVPR'19)*, 2019.

[10] A. Dosovitskiy, L. Beyer, A. Kolesnikov, D. Weissenborn, X. Zhai, T. Unterthiner, M. Dehghani, M. Minderer, G. Heigold, S. Gelly, J. Uszkoreit, and N. Houlsby. An Image is Worth 16x16 Words: Transformers for Image Recognition at Scale. In *Proceedings of the 9th International Conference on Learning Representations (ICLR'21)*, 2021.

[11] H. Drucker and Y. LeCun. Improving Generalization Performance Using Double Backpropagation. *IEEE Transactions on Neural Networks*, 3(6):991–997, 1992.

[12] P. Foret, A. Kleiner, H. Mobahi, and B. Neyshabur. Sharpness-aware Minimization for Efficiently Improving Generalization. In *Proceedings of the 9th International Conference on Learning Representations (ICLR'21)*, 2021.

[13] Z. Ge, F. Shang, H. Liu, Y. Liu, and X. Wang. Boosting Adversarial Transferability by Achieving Flat Local Maxima. *arXiv preprint arXiv:2306.05225*, 2023.

[14] J. Geiping, M. Goldblum, P. Pope, M. Moeller, and T. Goldstein. Stochastic Training is Not Necessary for Generalization. In *Proceedings of the 10th International Conference on Learning Representations (ICLR'22)*, 2022.

[15] J. Gilmer, L. Metz, F. Faghri, S. S. Schoenholz, M. Raghu, M. Wattenberg, and I. J. Goodfellow. Adversarial Spheres. In *Proceedings of the 6th International Conference on Learning Representations Workshops (ICLRW'18)*, 2018.

[16] M. Gubri, M. Cordy, M. Papadakis, Y. Le Traon, and K. Sen. Efficient and Transferable Adversarial Examples from Bayesian Neural Networks. In *Proceedings of the 38th Conference on Uncertainty in Artificial Intelligence (UAI'22)*, pages 738–748. PMLR, 2022.

[17] M. Gubri, M. Cordy, M. Papadakis, Y. L. Traon, and K. Sen. LGV: Boosting Adversarial Example Transferability from Large Geometric Vicinity. In *Proceedings of the 17th European Conference on Computer Vision (ECCV'22)*, pages 603–618, 2022.

[18] Y. Guo, Q. Li, and H. Chen. Backpropagating Linearly Improves Transferability of Adversarial Examples. In *Proceedings of the 34th Annual Conference on Neural Information Processing Systems (NeurIPS'20)*, pages 85–95, 2020.

[19] S. Hu, X. Liu, Y. Zhang, M. Li, L. Y. Zhang, H. Jin, and L. Wu. Protecting Facial Privacy: Generating Adversarial Identity Masks via Style-robust Makeup Transfer. In *Proceedings of the IEEE/CVF Conference on Computer Vision and Pattern Recognition (CVPR'22)*, pages 15014–15023, 2022.

[20] S. Hu, Y. Zhang, X. Liu, L. Y. Zhang, M. Li, and H. Jin. Advhash: Set-to-set Targeted Attack on Deep Hashing with One Single Adversarial Patch. In *Proceedings of the 29th ACM International Conference on Multimedia (MM'21)*, pages 2335–2343, 2021.

[21] D. Jakubovitz and R. Giryes. Improving DNN Robustness to Adversarial Attacks using Jacobian Regularization. In *Proceedings of 15th the European Conference on Computer Vision (ECCV'18)*, pages 514–529, 2018.

[22] R. Karakida, T. Takase, T. Hayase, and K. Osawa. Understanding Gradient Regularization in Deep Learning: Efficient Finite-Difference Computation and Implicit Bias. *arXiv preprint arXiv:2210.02720*, 2022.

[23] J. Kwon and S. Lee. Improving the Robustness of Model Compression by On-Manifold Adversarial Training. *Future Internet*, 13(12):300, 2021.

[24] M. Li, C. Deng, T. Li, J. Yan, X. Gao, and H. Huang. Towards Transferable Targeted Attack. In *Proceedings of the IEEE/CVF Conference on Computer Vision and Pattern Recognition (CVPR'20)*, 2020.

[25] Q. Li, Y. Guo, W. Zuo, and H. Chen. Making Substitute Models More Bayesian Can Enhance Transferability of Adversarial Examples. In *Proceedings of the 11th International Conference on Learning Representations (ICLR'23)*, 2023.

[26] Y. Li, S. Bai, Y. Zhou, C. Xie, Z. Zhang, and A. Yuille. Learning Transferable Adversarial Examples via Ghost Networks. In *Proceedings of the 34th AAAI Conference on Artificial Intelligence (AAAI'20)*, pages 11458–11465, 2020.

[27] W.-A. Lin, C. P. Lau, A. Levine, R. Chellappa, and S. Feizi. Dual Manifold Adversarial Robustness: Defense against Lp and non-Lp Adversarial Attacks. In *Proceedings of the 34th Annual Conference on Neural Information Processing Systems (NeurIPS'20)*, pages 3487–3498, 2020.

[28] Y. Liu, X. Chen, C. Liu, and D. Song. Delving into Transferable Adversarial Examples and Black-box Attacks. In *Proceedings of the 5th International Conference on Learning Representations (ICLR'17)*, 2017.

[29] X. Ma, B. Li, Y. Wang, S. M. Erfani, S. Wijewickrema, G. Schoenebeck, M. E. Houle, D. Song, and J. Bailey. Characterizing Adversarial Subspaces Using Local Intrinsic Dimensionality. In *Proceedings of the 6th International Conference on Learning Representations (ICLR'18)*, 2018.

[30] A. Madry, A. Makelov, L. Schmidt, D. Tsipras, and A. Vladu. Towards Deep Learning Models Resistant to Adversarial Attacks. In *Proceedings of the 6th International Conference on Learning Representations (ICLR'18)*, 2018.

[31] K. Mahmood, R. Mahmood, and M. van Dijk. On the Robustness of Vision Transformers to Adversarial Examples. In *Proceedings of IEEE/CVF International Conference on Computer Vision (ICCV'21)*, pages 7838–7847, 2021.

[32] Y. Mao, C. Fu, S. Wang, S. Ji, X. Zhang, Z. Liu, J. Zhou, A. Liu, R. Beyah, and T. Wang. Transfer Attacks Revisited: A Large-Scale Empirical Study in Real Computer Vision Settings. In *Proceedings of the 43rd IEEE Symposium on Security and Privacy (S&P'22)*, pages 1423–1439, 2022.

[33] J. Martens, I. Sutskever, and K. Swersky. Estimating the Hessian by Back-propagating Curvature. In *Proceedings of the 29th International Conference on Machine Learning (ICML'12)*, pages 963–970, 2012.

[34] T. Möllenhoff and M. E. Khan. SAM as an Optimal Relaxation of Bayes. In *Proceedings of the 11th International Conference on Learning Representations (ICLR'23)*, 2023.

[35] M. Naseer, S. Khan, M. Hayat, F. S. Khan, and F. Porikli. On Generating Transferable Targeted Perturbations. In *Proceedings of the 2021 IEEE/CVF International Conference on Computer Vision (ICCV'21)*, pages 7708–7717, 2021.

[36] M. Naseer, K. Ranasinghe, S. Khan, F. Khan, and F. Porikli. On Improving Adversarial Transferability of Vision Transformers. In *Proceedings of the 10th International Conference on Learning Representations (ICLR'22)*, 2022.

[37] K. Patel, W. Beluch, D. Zhang, M. Pfeiffer, and B. Yang. On-manifold Adversarial Data Augmentation Improves Uncertainty Calibration. In *Proceedings of the 25th International Conference on Pattern Recognition (ICPR'20)*, pages 8029–8036, 2020.

[38] Z. Qin, Y. Fan, Y. Liu, L. Shen, Y. Zhang, J. Wang, and B. Wu. Boosting the Transferability of Adversarial Attacks with Reverse Adversarial Perturbation. In *Proceedings of the 36th Annual Conference on Neural Information Processing Systems (NeurIPS'22)*, 2022.

[39] A. Ross and F. Doshi-Velez. Improving the Adversarial Robustness and Interpretability of Deep Neural Networks by Regularizing Their Input Gradients. In *Proceedings of the 32nd AAAI Conference on Artificial Intelligence (AAAI'18)*, 2018.

[40] K. Roth, Y. Kilcher, and T. Hofmann. Adversarial Training Is A Form of Data-dependent Operator Norm Regularization. In *Proceedings of the 34th Annual Conference on Neural Information Processing Systems (NeurIPS'20)*, volume 33, pages 14973–14985, 2020.

[41] R. Shao, Z. Shi, J. Yi, P.-Y. Chen, and C.-j. Hsieh. On the Adversarial Robustness of Vision Transformers. In *Proceedings of the 36th Annual Conference on Neural Information Processing Systems (NeurIPS'22)*, 2022.

[42] S. L. Smith, B. Dherin, D. Barrett, and S. De. On the Origin of Implicit Regularization in Stochastic Gradient Descent. In *Proceedings of the 9th International Conference on Learning Representations (ICLR'21)*, 2021.

[43] Y. Song, T. Kim, S. Nowozin, S. Ermon, and N. Kushman. PixelDefend: Leveraging Generative Models to Understand and Defend against Adversarial Examples. In *Proceedings of the 6th International Conference on Learning Representations (ICLR'18)*, 2018.

[44] J. Springer, M. Mitchell, and G. Kenyon. A Little Robustness Goes a Long Way: Leveraging Robust Features for Targeted Transfer Attacks. In *Proceedings of the 35th Annual Conference on Neural Information Processing Systems (NeurIPS'21)*, pages 9759–9773, 2021.

[45] J. M. Springer, M. Mitchell, and G. T. Kenyon. Uncovering Universal Features: How Adversarial Training Improves Adversarial Transferability. In *International Conference on Machine Learning Workshop (ICMLW'21) on Adversarial Machine Learning*, 2021.

[46] D. Stutz, M. Hein, and B. Schiele. Disentangling Adversarial Robustness and Generalization. In *Proceedings of the IEEE/CVF Conference on Computer Vision and Pattern Recognition (CVPR'19)*, 2019.

[47] C. Szegedy, V. Vanhoucke, S. Ioffe, J. Shlens, and Z. Wojna. Rethinking the Inception Architecture for Computer Vision. In *Proceedings of the IEEE Conference on Computer Vision and Pattern Recognition (CVPR'16)*, pages 2818–2826, 2016.

[48] C. Szegedy, W. Zaremba, I. Sutskever, J. Bruna, D. Erhan, I. Goodfellow, and R. Fergus. Intriguing Properties of Neural Networks. *arXiv preprint arXiv:1312.6199*, 2013.
[49] X. Wang, K. Tong, and K. He. Rethinking the Backward Propagation for Adversarial Transferability. *arXiv preprint arXiv:2306.12685*, 2023.
[50] Y. Wang and F. Farnia. On the Role of Generalization in Transferability of Adversarial Examples. *arXiv preprint arXiv:2206.09238*, 2022.
[51] K. Wen, T. Ma, and Z. Li. How Does Sharpness-Aware Minimization Minimize Sharpness? In *Proceedings of the 11th International Conference on Learning Representations (ICLR'23)*, 2023.
[52] R. Wightman. PyTorch Image Models. https://github.com/rwightman/pytorch-image-models, 2019.
[53] D. Wu, Y. Wang, S.-T. Xia, J. Bailey, and X. Ma. Skip Connections Matter: On the Transferability of Adversarial Examples Generated with ResNets. In *Proceedings of the 8th International Conference on Learning Representations (ICLR'20)*, 2020.
[54] T. Wu, T. Luo, and D. C. Wunsch. GNP Attack: Transferable Adversarial Examples via Gradient Norm Penalty. *arXiv preprint arXiv:2307.04099*, 2023.
[55] J. Xiao, L. Yang, Y. Fan, J. Wang, and Z.-Q. Luo. Understanding Adversarial Robustness Against On-manifold Adversarial Examples. *arXiv preprint arXiv:2210.00430*, 2022.
[56] C. Xie, Z. Zhang, Y. Zhou, S. Bai, J. Wang, Z. Ren, and A. L. Yuille. Improving Transferability of Adversarial Examples with Input Diversity. In *Proceedings of the IEEE/CVF Conference on Computer Vision and Pattern Recognition (CVPR'19)*, pages 2730–2739, 2019.
[57] X. Xu, J. Y. Zhang, E. Ma, H. H. Son, S. Koyejo, and B. Li. Adversarially Robust Models may not Transfer Better: Sufficient Conditions for Domain Transferability from the View of Regularization. In *Proceedings of the 39th International Conference on Machine Learning (ICML'22)*, pages 24770–24802. PMLR, 2022.
[58] Z. Yang, L. Li, X. Xu, S. Zuo, Q. Chen, P. Zhou, B. Rubinstein, C. Zhang, and B. Li. TRS: Transferability Reduced Ensemble via Promoting Gradient Diversity and Model Smoothness. In *Proceedings of the 35th Annual Conference on Neural Information Processing Systems (NeurIPS'21)*, pages 17642–17655, 2021.
[59] Y. Yoshida and T. Miyato. Spectral Norm Regularization for Improving the Generalizability of Deep Learning. *arXiv preprint arXiv:1705.10941*, 2017.
[60] S. Yun, D. Han, S. J. Oh, S. Chun, J. Choe, and Y. Yoo. CutMix: Regularization Strategy to Train Strong Classifiers with Localizable Features. In *Proceedings of the IEEE/CVF International Conference on Computer Vision (ICCV'19)*, pages 6023–6032, 2019.
[61] H. Zhang, M. Cisse, Y. N. Dauphin, and D. Lopez-Paz. Mixup: Beyond Empirical Risk Minimization. In *Proceedings of the 35th International Conference on Learning Representations (ICLR'18)*, 2018.
[62] Y. Zhao, H. Zhang, and X. Hu. Penalizing Gradient Norm for Efficiently Improving Generalization in Deep Learning. In *Proceedings of the 39th International Conference on Machine Learning (ICML'22)*, 2022.
[63] Z. Zhao, Z. Liu, and M. Larson. On Success and Simplicity: A Second Look at Transferable Targeted Attacks. In *Proceedings of the 35th Annual Conference Neural Information Processing Systems (NeurIPS'21)*, pages 6115–6128, 2021.
[64] Z. Zhou, S. Hu, R. Zhao, Q. Wang, L. Y. Zhang, J. Hou, and H. Jin. Downstream-agnostic Adversarial Examples. In *Proceedings of the IEEE/CVF International Conference on Computer Vision (ICCV'23)*, 2023.

Appendix A. Supplemental Materials

A.1. Experimental Settings

Tab. 11 reports the detailed training settings. Code and models are available at https://github.com/CGCL-codes/TransferAttackSurrogates.

A.2. Proof of Transferability Lower Bound

Here we present the proof of Theorem 1. The following two lemmas are used in the proof.

Lemma 1. *For arbitrary vector δ, x, y, suppose $\|\delta\|_2 \leq \epsilon, x$ and y are unit vectors, i.e., $\|x\|_2 = \|y\|_2 = 1$. Let $\cos\langle x, y\rangle = \frac{x \cdot y}{\|x\|_2 \cdot \|y\|_2}$. Let c denote any real number. Then*

$$\delta \cdot y < c - \epsilon\sqrt{2 - 2\cos\langle x, y\rangle} \Rightarrow \delta \cdot x < c. \quad (3)$$

Proof. $\delta \cdot x = \delta \cdot y + \delta \cdot (x - y) < c - \epsilon\sqrt{2 - 2\cos\langle x, y\rangle} + \delta \cdot (x - y)$. By law of cosines, $\delta \cdot (x - y) \leq \|\delta\|_2 \cdot \|(x - y)\|_2 \leq \epsilon\sqrt{2 - 2\cos\langle x, y\rangle}$. Hence, $\delta \cdot x < c$ $\square$

Lemma 2. *For arbitrary events A and B, we have $\Pr(\neg A \cap \neg B) \geq 1 - \Pr(A) - \Pr(B)$, where $\Pr(\cdot)$ denotes the probability of a event.*

Proof. For events A and B, we have $\Pr(A \cup B) + \Pr(\neg(A \cup B)) = 1$. And it is true that $\Pr(A) + \Pr(B) \geq \Pr(A \cup B)$ and $\neg(A \cup B) = \neg A \cap \neg B$. Then we have $\Pr(A) + \Pr(B) + \Pr(\neg A \cap \neg B) \geq \Pr(A \cup B) + \Pr(\neg(A \cup B)) = 1$, thus $\Pr(\neg A \cap \neg B) \geq 1 - \Pr(A) - \Pr(B)$. $\square$

Note that this is a generalizable property. Given any number of events $A_1, A_2, ..., A_n$, we can also have $\Pr(A_1) + \Pr(A_2) + ... + \Pr(A_n) + \Pr(\neg A_1 \cap \neg A_2 ... \cap \neg A_n) \geq 1$, thus $\Pr(\neg A_1 \cap \neg A_2 ... \neg A_n) \geq 1 - \Pr(A_1) - \Pr(A_2) - ... - \Pr(A_n)$.

Proof for Theorem 1. The proof builds upon the derivations in Yang *et al.* [58], with the primary modifications focusing on the definition of smoothness. We omit some intermediate steps to save space.

TABLE 11: Hyperparameters for training on CIFAR-10 and ImageNette. *MU*, *CM*, *CO*, and *LS* refer to the X-axis parameters of Figs. 5 to 8. *AT* refer to Figs. 2 to 4. *IR*, *JR*, *ER*, and *SAM* refer to Figs. 9 and 10, respectively. The bold items in parameter lists correspond to Tabs. 2 and 3.

	CIFAR-10	**ImageNette**
Surrogate Architecture	ResNet18	ResNet50
Input size	32×32	224×224
Batch size	128	128
Epoch	200	50
Warmup epoch	10	5
Finetune	False	True
Peak learning rate	0.1	1
Learning rate decay	cosine	
Optimizer	SGD	
(*MU*) **p**	{**0.1**, 0.3, 0.5, 0.7, **0.9**}	
(*CM*) **p**	{**0.1**, 0.3, 0.5, 0.7, **0.9**}	
(*CO*) M	{**8**, 12, 16, 20, **24**}	{**80**, 100, 120, 140, **160**}
(*LS*) p	{**0.1**, 0.2, 0.3, 0.4, **0.5**}	
(*AT*) Step	10	5
(*AT*) Step_size	$0.25 \times \epsilon$	$0.4 \times \epsilon$
(*AT*) ϵ	{0.01, **0.03**, 0.05, 0.1, 0.2, 0.5, 1}	{0.05, 0.1, 0.2, 0.5, **1**, 3, 5}
(*IR*) λ_{ir}	{0.1, 0.3, **0.5**, 0.7, 1}	{0.1, 0.5, **1**, 1.5, 2}
(*JR*) λ_{jr}	{1e-5, **1e-4**, 0.01, 0.05, 0.1}	{0.001, 0.01, **0.1**, 0.5, 1}
(*ER*) λ_{er}	{1e-3, 5e-3, 0.01, **0.05**, 0.1}	{**0.05**, 0.3, 0.5, 0.7, 1}
(*SAM*) ρ	{0.01, 0.05, **0.1**, 0.15, 0.2}	{**0.2**, 0.5, 1, 2, 3}

TABLE 12: Clean accuracy of models in Tabs. 2, 3 and 10. We report the results of a fixed random seed here.

	CIFAR10		ImageNette	
	Clean Acc Train/Test	Generalization Gap (↓)	Clean Acc Train/Test	Generalization Gap (↓)
ST	100.00/94.40	5.60	97.75/96.74	1.01
MU, $\tau = 1$	100.00/95.04	4.96	95.53/97.10	-1.57
MU, $\tau = 5$	**100.00/96.13**	**3.87**	**84.23/97.58**	**-13.35**
CM, $\tau = 1$	100.00/95.45	4.55	94.84/97.10	-2.26
CM, $\tau = 5$	**99.99/95.93**	**4.06**	**82.46/97.73**	**-15.27**
CO, $\tau = 1$	100.00/95.09	4.91	97.40/96.94	0.46
CO, $\tau = 5$	100.00/95.79	4.21	95.41/96.97	-1.56
LS, $\tau = 1$	100.00/94.84	5.16	98.09/97.48	0.61
LS, $\tau = 5$	100.00/94.35	5.65	98.38/98.04	0.34
AT	100.00/94.30	5.70	96.15/95.99	0.16
IR	100.00/92.76	7.24	97.24/96.13	1.11
JR	100.00/94.46	5.54	97.51/96.28	1.23
ER	100.00/92.83	7.17	97.86/97.12	0.74
SAM	100.00/95.20	4.80	96.54/97.53	-0.99
SAM&IR	99.87/92.72	7.15	95.49/96.51	-1.02
SAM&JR	100.00/95.16	4.84	95.62/96.79	-1.17

TABLE 13: Transfer ASRs (in %) of AEs crafted against different surrogates on **CIFAR-10** and **ImageNette** using **AutoAttack**. We plot this table in the same way as Tab. 2.

CIFAR-10

	4/255				8/255				16/255			
	ResNet50	VGG16	InceptionV3	DenseNet121	ResNet50	VGG16	InceptionV3	DenseNet121	ResNet50	VGG16	InceptionV3	DenseNet121
ST	$41.2_{\pm 5.6}$	$30.1_{\pm 3.5}$	$41.7_{\pm 5.3}$	$58.6_{\pm 7.1}$	$62.9_{\pm 7.9}$	$54.5_{\pm 6.5}$	$64.8_{\pm 6.0}$	$80.5_{\pm 6.8}$	$83.2_{\pm 5.2}$	$81.0_{\pm 5.5}$	$84.2_{\pm 3.8}$	$91.0_{\pm 3.3}$
MU, $\tau=1$	$27.9_{\pm 5.1}$	$20.9_{\pm 2.5}$	$29.0_{\pm 4.8}$	$40.2_{\pm 7.0}$	$48.5_{\pm 6.9}$	$40.6_{\pm 3.7}$	$51.4_{\pm 5.9}$	$65.3_{\pm 7.5}$	$73.1_{\pm 6.4}$	$71.3_{\pm 4.5}$	$76.5_{\pm 4.7}$	$85.2_{\pm 5.1}$
MU, $\tau=3$	$20.4_{\pm 0.6}$	$16.4_{\pm 0.5}$	$23.3_{\pm 1.2}$	$27.8_{\pm 1.6}$	$37.7_{\pm 0.9}$	$31.2_{\pm 1.1}$	$42.0_{\pm 1.4}$	$51.1_{\pm 1.3}$	$68.0_{\pm 1.9}$	$64.7_{\pm 1.7}$	$72.9_{\pm 1.2}$	$80.4_{\pm 1.2}$
MU, $\tau=5$	$18.8_{\pm 0.3}$	$15.7_{\pm 0.3}$	$20.8_{\pm 1.0}$	$24.5_{\pm 0.8}$	$33.8_{\pm 1.7}$	$28.6_{\pm 0.9}$	$37.5_{\pm 1.0}$	$44.9_{\pm 1.6}$	$64.1_{\pm 1.5}$	$60.5_{\pm 1.9}$	$68.3_{\pm 0.4}$	$76.4_{\pm 1.5}$
CM, $\tau=1$	$22.4_{\pm 0.9}$	$16.7_{\pm 1.3}$	$21.8_{\pm 0.6}$	$30.3_{\pm 1.3}$	$39.6_{\pm 1.7}$	$32.42_{\pm .5}$	$39.0_{\pm 1.0}$	$53.4_{\pm 2.5}$	$64.5_{\pm 2.0}$	$62.4_{\pm 3.2}$	$64.9_{\pm 1.7}$	$77.8_{\pm 3.2}$
CM, $\tau=3$	$14.3_{\pm 1.2}$	$11.5_{\pm 0.4}$	$14.2_{\pm 1.1}$	$17.2_{\pm 2.0}$	$25.8_{\pm 3.0}$	$20.2_{\pm 1.8}$	$25.1_{\pm 2.6}$	$32.1_{\pm 4.4}$	$48.9_{\pm 4.1}$	$47.1_{\pm 2.7}$	$49.8_{\pm 3.0}$	$60.6_{\pm 4.6}$
CM, $\tau=5$	$12.3_{\pm 0.5}$	$10.4_{\pm 0.2}$	$12.0_{\pm 1.1}$	$13.7_{\pm 1.2}$	$21.9_{\pm 1.3}$	$17.5_{\pm 0.6}$	$21.3_{\pm 0.9}$	$26.5_{\pm 1.8}$	$44.4_{\pm 1.6}$	$41.5_{\pm 1.6}$	$44.3_{\pm 1.9}$	$53.4_{\pm 1.8}$
CO, $\tau=1$	$40.7_{\pm 7.0}$	$31.1_{\pm 7.0}$	$39.8_{\pm 5.9}$	$55.9_{\pm 8.1}$	$62.4_{\pm 6.9}$	$55.3_{\pm 8.1}$	$63.1_{\pm 6.2}$	$78.2_{\pm 5.9}$	$82.5_{\pm 5.6}$	$79.9_{\pm 6.3}$	$82.8_{\pm 5.3}$	$89.9_{\pm 3.7}$
CO, $\tau=3$	$34.6_{\pm 5.2}$	$24.9_{\pm 2.8}$	$33.7_{\pm 5.1}$	$47.1_{\pm 8.0}$	$55.5_{\pm 5.8}$	$46.0_{\pm 4.7}$	$55.8_{\pm 6.7}$	$70.7_{\pm 8.0}$	$79.6_{\pm 5.4}$	$74.4_{\pm 5.1}$	$79.2_{\pm 5.6}$	$86.8_{\pm 5.0}$
CO, $\tau=5$	$30.8_{\pm 2.5}$	$22.3_{\pm 2.0}$	$31.0_{\pm 3.3}$	$42.1_{\pm 6.7}$	$49.5_{\pm 5.0}$	$41.3_{\pm 4.8}$	$51.3_{\pm 5.8}$	$63.9_{\pm 7.8}$	$73.2_{\pm 5.6}$	$69.3_{\pm 6.3}$	$74.5_{\pm 6.4}$	$81.7_{\pm 7.0}$
LS, $\tau=1$	$35.5_{\pm 4.8}$	$28.2_{\pm 5.7}$	$35.5_{\pm 3.3}$	$48.4_{\pm 5.7}$	$54.3_{\pm 9.4}$	$49.7_{\pm 10.7}$	$56.0_{\pm 6.4}$	$69.4_{\pm 8.4}$	$76.1_{\pm 7.8}$	$76.9_{\pm 8.3}$	$78.3_{\pm 6.0}$	$85.9_{\pm 5.1}$
LS, $\tau=3$	$34.2_{\pm 7.5}$	$27.3_{\pm 4.6}$	$33.9_{\pm 5.6}$	$44.1_{\pm 2.8}$	$55.0_{\pm 13.6}$	$50.0_{\pm 10.0}$	$55.9_{\pm 11.0}$	$68.2_{\pm 5.9}$	$76.8_{\pm 12.1}$	$76.6_{\pm 10.0}$	$78.3_{\pm 9.3}$	$85.5_{\pm 5.3}$
LS, $\tau=5$	$31.3_{\pm 3.5}$	$26.6_{\pm 3.5}$	$30.2_{\pm 3.1}$	$41.2_{\pm 2.9}$	$51.1_{\pm 8.2}$	$48.6_{\pm 8.0}$	$51.2_{\pm 6.9}$	$65.6_{\pm 7.0}$	$72.2_{\pm 7.7}$	$74.5_{\pm 8.2}$	$73.5_{\pm 6.2}$	$83.3_{\pm 5.4}$
AT	$54.4_{\pm 2.3}$	$45.3_{\pm 1.5}$	$49.5_{\pm 3.6}$	$61.0_{\pm 3.5}$	$80.2_{\pm 5.8}$	$73.7_{\pm 5.9}$	$77.5_{\pm 4.1}$	$86.4_{\pm 4.2}$	$90.8_{\pm 3.0}$	$89.5_{\pm 3.2}$	$89.8_{\pm 2.8}$	$92.9_{\pm 2.3}$
IR	$51.9_{\pm 1.4}$	$45.3_{\pm 1.1}$	$48.0_{\pm 0.6}$	$54.4_{\pm 1.1}$	$85.9_{\pm 3.4}$	$82.4_{\pm 3.9}$	$83.8_{\pm 3.3}$	$87.4_{\pm 3.2}$	$92.4_{\pm 2.1}$	$92.2_{\pm 2.3}$	$91.8_{\pm 2.1}$	$92.0_{\pm 2.0}$
JR	$63.5_{\pm 8.7}$	$53.1_{\pm 7.1}$	$62.4_{\pm 5.7}$	$75.1_{\pm 4.5}$	$78.9_{\pm 6.8}$	$73.7_{\pm 6.1}$	$79.5_{\pm 4.1}$	$88.7_{\pm 2.6}$	$87.6_{\pm 4.3}$	$87.2_{\pm 3.9}$	$88.1_{\pm 2.4}$	$92.1_{\pm 2.1}$
ER	$55.0_{\pm 5.5}$	$42.9_{\pm 5.6}$	$46.2_{\pm 7.4}$	$55.2_{\pm 13.8}$	$82.3_{\pm 5.5}$	$74.1_{\pm 7.9}$	$76.1_{\pm 8.8}$	$81.1_{\pm 12.2}$	$90.6_{\pm 4.0}$	$89.3_{\pm 4.6}$	$88.9_{\pm 4.0}$	$89.8_{\pm 4.4}$
SAM	$66.1_{\pm 8.6}$	$53.4_{\pm 5.8}$	$66.0_{\pm 8.8}$	$81.1_{\pm 6.9}$	$88.4_{\pm 4.7}$	$83.4_{\pm 4.5}$	$88.7_{\pm 4.8}$	$94.1_{\pm 2.4}$	$94.3_{\pm 3.0}$	$94.0_{\pm 3.0}$	$94.2_{\pm 2.9}$	$94.8_{\pm 2.4}$
SAM&IR	$52.9_{\pm 0.6}$	$47.0_{\pm 1.0}$	$48.2_{\pm 1.2}$	$54.1_{\pm 1.7}$	$88.3_{\pm 2.3}$	$85.5_{\pm 2.7}$	$85.7_{\pm 2.4}$	$88.7_{\pm 2.0}$	$92.8_{\pm 2.0}$	$92.9_{\pm 2.0}$	$92.2_{\pm 2.0}$	$92.4_{\pm 1.9}$
SAM&JR	$69.8_{\pm 3.0}$	$57.2_{\pm 2.9}$	$69.2_{\pm 2.5}$	$82.7_{\pm 2.1}$	$90.4_{\pm 3.9}$	$86.2_{\pm 4.7}$	$90.3_{\pm 3.5}$	$94.6_{\pm 1.8}$	$94.8_{\pm 1.9}$	$94.6_{\pm 2.1}$	$94.6_{\pm 1.7}$	$94.9_{\pm 1.6}$

ImageNette

	4/255				8/255				16/255			
	VGG16	DenseNet121	MobileNetV2	Xception	VGG16	DenseNet121	MobileNetV2	Xception	VGG16	DenseNet121	MobileNetV2	Xception
ST	$10.1_{\pm 0.7}$	$16.0_{\pm 1.0}$	$7.1_{\pm 0.5}$	$6.7_{\pm 0.1}$	$27.4_{\pm 3.0}$	$41.0_{\pm 2.8}$	$17.7_{\pm 0.7}$	$16.9_{\pm 1.1}$	$61.5_{\pm 6.5}$	$83.3_{\pm 4.9}$	$51.5_{\pm 2.7}$	$44.8_{\pm 4.6}$
MU, $\tau=1$	$7.9_{\pm 1.5}$	$11.1_{\pm 1.1}$	$5.9_{\pm 0.5}$	$6.1_{\pm 0.5}$	$20.3_{\pm 1.5}$	$23.6_{\pm 2.2}$	$13.5_{\pm 1.3}$	$11.1_{\pm 0.3}$	$43.8_{\pm 0.8}$	$60.5_{\pm 4.5}$	$39.1_{\pm 2.3}$	$29.5_{\pm 1.9}$
MU, $\tau=3$	$6.8_{\pm 0.4}$	$7.8_{\pm 0.6}$	$5.1_{\pm 0.5}$	$5.5_{\pm 0.5}$	$13.3_{\pm 0.9}$	$14.3_{\pm 0.9}$	$8.7_{\pm 0.9}$	$9.0_{\pm 0.8}$	$30.8_{\pm 2.8}$	$35.6_{\pm 1.6}$	$26.4_{\pm 2.2}$	$19.3_{\pm 1.7}$
MU, $\tau=5$	$5.9_{\pm 0.5}$	$7.0_{\pm 0.2}$	$4.2_{\pm 0.4}$	$5.3_{\pm 0.3}$	$10.4_{\pm 1.0}$	$11.6_{\pm 0.6}$	$8.2_{\pm 0.6}$	$7.5_{\pm 0.5}$	$24.9_{\pm 0.9}$	$27.3_{\pm 1.1}$	$20.7_{\pm 1.3}$	$17.2_{\pm 0.8}$
CM, $\tau=1$	$7.3_{\pm 0.7}$	$9.1_{\pm 1.1}$	$5.3_{\pm 0.3}$	$5.7_{\pm 0.3}$	$15.3_{\pm 0.7}$	$17.9_{\pm 1.5}$	$9.3_{\pm 0.7}$	$8.6_{\pm 0.4}$	$33.1_{\pm 1.7}$	$44.0_{\pm 3.6}$	$25.6_{\pm 2.0}$	$18.7_{\pm 0.9}$
CM, $\tau=3$	$5.8_{\pm 0.4}$	$6.4_{\pm 0.6}$	$4.2_{\pm 0.6}$	$5.3_{\pm 0.3}$	$9.3_{\pm 0.9}$	$11.4_{\pm 1.2}$	$7.1_{\pm 1.1}$	$6.9_{\pm 0.5}$	$20.2_{\pm 0.8}$	$24.7_{\pm 2.3}$	$17.2_{\pm 0.6}$	$12.7_{\pm 1.7}$
CM, $\tau=5$	$4.5_{\pm 0.3}$	$5.7_{\pm 0.5}$	$3.8_{\pm 0.4}$	$4.7_{\pm 0.3}$	$7.9_{\pm 0.5}$	$8.5_{\pm 0.7}$	$5.7_{\pm 0.3}$	$6.3_{\pm 0.7}$	$16.6_{\pm 1.0}$	$16.9_{\pm 0.9}$	$14.7_{\pm 1.3}$	$9.9_{\pm 0.7}$
CO, $\tau=1$	$10.9_{\pm 1.1}$	$15.3_{\pm 0.7}$	$6.9_{\pm 0.7}$	$7.2_{\pm 0.0}$	$26.7_{\pm 2.5}$	$41.3_{\pm 3.5}$	$17.9_{\pm 0.7}$	$16.3_{\pm 1.1}$	$60.2_{\pm 4.6}$	$83.9_{\pm 4.1}$	$50.6_{\pm 3.4}$	$43.1_{\pm 3.1}$
CO, $\tau=3$	$10.3_{\pm 1.5}$	$14.6_{\pm 0.2}$	$7.2_{\pm 0.4}$	$7.6_{\pm 0.4}$	$26.3_{\pm 1.9}$	$40.3_{\pm 2.3}$	$18.9_{\pm 0.9}$	$15.7_{\pm 3.3}$	$59.6_{\pm 3.4}$	$82.4_{\pm 1.6}$	$51.2_{\pm 5.4}$	$42.1_{\pm 4.3}$
CO, $\tau=5$	$9.7_{\pm 1.3}$	$13.2_{\pm 0.4}$	$6.2_{\pm 1.0}$	$6.6_{\pm 0.4}$	$24.4_{\pm 3.2}$	$35.4_{\pm 4.6}$	$14.8_{\pm 0.8}$	$15.0_{\pm 0.4}$	$58.2_{\pm 5.4}$	$79.9_{\pm 2.1}$	$47.1_{\pm 3.9}$	$39.8_{\pm 1.6}$
LS, $\tau=1$	$5.9_{\pm 0.7}$	$7.7_{\pm 0.3}$	$4.7_{\pm 0.9}$	$5.2_{\pm 0.2}$	$11.1_{\pm 1.1}$	$14.2_{\pm 1.0}$	$8.1_{\pm 0.5}$	$7.9_{\pm 0.3}$	$24.8_{\pm 0.8}$	$32.8_{\pm 0.6}$	$22.8_{\pm 1.6}$	$15.5_{\pm 0.9}$
LS, $\tau=3$	$4.9_{\pm 0.3}$	$6.4_{\pm 0.2}$	$4.1_{\pm 0.7}$	$5.2_{\pm 0.4}$	$9.5_{\pm 0.3}$	$11.7_{\pm 0.7}$	$7.3_{\pm 0.3}$	$7.1_{\pm 0.3}$	$22.0_{\pm 0.6}$	$26.6_{\pm 1.0}$	$19.4_{\pm 0.8}$	$14.3_{\pm 1.9}$
LS, $\tau=5$	$5.1_{\pm 0.5}$	$5.7_{\pm 0.5}$	$3.9_{\pm 0.1}$	$4.8_{\pm 0.0}$	$8.6_{\pm 1.8}$	$9.6_{\pm 1.2}$	$6.5_{\pm 0.7}$	$6.9_{\pm 0.9}$	$18.1_{\pm 2.5}$	$22.8_{\pm 0.2}$	$17.2_{\pm 2.2}$	$14.1_{\pm 0.5}$
AT	$11.3_{\pm 0.9}$	$15.7_{\pm 0.9}$	$11.4_{\pm 0.6}$	$11.1_{\pm 0.3}$	$50.3_{\pm 5.9}$	$68.9_{\pm 2.5}$	$57.8_{\pm 5.0}$	$51.6_{\pm 3.6}$	$94.9_{\pm 0.7}$	$97.1_{\pm 0.3}$	$95.5_{\pm 1.1}$	$93.8_{\pm 0.8}$
IR	$19.1_{\pm 6.1}$	$29.9_{\pm 6.3}$	$16.7_{\pm 5.1}$	$16.7_{\pm 4.7}$	$60.7_{\pm 14.7}$	$82.7_{\pm 9.5}$	$64.1_{\pm 16.7}$	$55.9_{\pm 13.5}$	$91.2_{\pm 7.6}$	$96.2_{\pm 0.8}$	$92.0_{\pm 5.6}$	$90.3_{\pm 6.5}$
JR	$23.4_{\pm 2.2}$	$37.3_{\pm 2.3}$	$20.0_{\pm 1.8}$	$19.1_{\pm 1.1}$	$67.3_{\pm 3.5}$	$88.2_{\pm 0.5}$	$66.6_{\pm 1.8}$	$57.7_{\pm 3.5}$	$93.1_{\pm 1.5}$	$97.4_{\pm 0.4}$	$93.5_{\pm 0.3}$	$91.9_{\pm 1.1}$
ER	$12.1_{\pm 2.7}$	$19.6_{\pm 2.4}$	$7.5_{\pm 0.5}$	$8.1_{\pm 1.5}$	$32.5_{\pm 9.3}$	$51.9_{\pm 9.5}$	$22.1_{\pm 4.5}$	$21.5_{\pm 5.5}$	$65.7_{\pm 17.9}$	$89.2_{\pm 5.2}$	$55.0_{\pm 8.4}$	$50.1_{\pm 11.9}$
SAM	$22.6_{\pm 2.6}$	$30.1_{\pm 0.5}$	$12.7_{\pm 0.5}$	$11.5_{\pm 0.1}$	$55.5_{\pm 1.9}$	$72.5_{\pm 3.1}$	$39.4_{\pm 3.4}$	$34.8_{\pm 3.0}$	$89.8_{\pm 1.0}$	$97.1_{\pm 0.7}$	$86.1_{\pm 10.3}$	$82.0_{\pm 13.8}$
SAM&IR	$23.7_{\pm 4.1}$	$37.5_{\pm 2.3}$	$22.0_{\pm 2.8}$	$19.7_{\pm 1.5}$	$68.9_{\pm 8.3}$	$91.1_{\pm 2.3}$	$73.5_{\pm 6.9}$	$64.3_{\pm 7.5}$	$94.6_{\pm 1.3}$	$96.9_{\pm 0.5}$	$95.4_{\pm 1.2}$	$94.1_{\pm 1.3}$
SAM&JR	$32.7_{\pm 4.5}$	$47.3_{\pm 3.1}$	$27.1_{\pm 3.3}$	$24.9_{\pm 3.3}$	$74.3_{\pm 7.3}$	$92.7_{\pm 1.5}$	$72.8_{\pm 7.0}$	$65.3_{\pm 8.7}$	$95.1_{\pm 3.1}$	$98.4_{\pm 0.6}$	$95.0_{\pm 3.0}$	$93.5_{\pm 2.7}$

Proof. Define auxiliary function f, $g : \mathcal{M} \times \mathcal{L} \to \mathbb{R}$ such that

$$f(x,y) = \frac{\min_{y' \in \mathcal{L}: y' \neq y} \ell_{\mathcal{F}}(x+\delta, y') - \ell_{\mathcal{F}}(x,y) - \overline{\sigma}_{\mathcal{F}} \epsilon^2/2}{\|\nabla_x \ell_{\mathcal{F}}(x,y)\|_2},$$
$$g(x,y) = \frac{\min_{y' \in \mathcal{L}: y' \neq y} \ell_{\mathcal{G}}(x+\delta, y') - \ell_{\mathcal{G}}(x,y) + \overline{\sigma}_{\mathcal{G}} \epsilon^2/2}{\|\nabla_x \ell_{\mathcal{G}}(x,y)\|_2}. \tag{4}$$

The f and g are orthogonal to the confidence score functions of model $\mathcal{F}$ and $\mathcal{G}$, we reuse the notation f here. Note that $c_{\mathcal{F}} = \min_{(x,y)\sim\mathcal{D}} f(x,y), c_{\mathcal{G}} = \max_{(x,y)\sim\mathcal{D}} g(x,y)$.

Observing Definition 3, the transferability concerns a successful transfer requiring 4 events, *i.e.*, $\mathcal{F}(x) = y, \mathcal{G}(x) = y$, $\mathcal{F}(x+\delta) \neq y$, and $\mathcal{G}(x+\delta) \neq y$. In other words, both $\mathcal{F}$ and $\mathcal{G}$ give the correct prediction for x, and the wrong prediction for $x+\delta$, we have:

$$\begin{aligned} &\Pr\left(T_r(\mathcal{F},\mathcal{G},x,y)=1\right) \\ =&\Pr\left(\mathcal{F}(x)=y \cap \mathcal{G}(x)=y \cap \mathcal{F}(x+\delta) \neq y \cap \mathcal{G}(x+\delta) \neq y\right) \\ \geq& 1 - \Pr(\mathcal{F}(x) \neq y) - \Pr(\mathcal{G}(x) \neq y) - \Pr\left(\mathcal{F}(x+\delta)=y\right) \\ &- \Pr\left(\mathcal{G}(x+\delta)=y\right) \\ \geq& 1 - \gamma_{\mathcal{F}} - \gamma_{\mathcal{G}} - \alpha - \Pr\left(\mathcal{G}(x+\delta)=y\right). \end{aligned} \tag{5}$$

Here we use the general version for 4 events of Lemma 2 to derive the first inequality. Note that $\mathcal{F}(x) \neq y, \mathcal{G}(x) \neq y$, $\mathcal{F}(x+\delta) = y$ and $\mathcal{G}(x+\delta) = y$ are the corresponding complementary events of $\mathcal{F}(x) = y$, $\mathcal{G}(x) = y$, $\mathcal{F}(x+\delta) \neq y$, and $\mathcal{G}(x+\delta) \neq y$. In the second inequality, we use the definitions of the model risks $\gamma_{\mathcal{F}}$, $\gamma_{\mathcal{G}}$, and α ($\Pr\left(\mathcal{F}(x+\delta)=y\right) < \alpha$ holds, see Theorem 1).

Given that model predicts the label for which training loss is minimized, $\mathcal{F}(x+\delta) = y \iff \ell_{\mathcal{F}}(x+\delta, y) < \min_{y' \in \mathcal{L}: y' \neq y} \ell_{\mathcal{F}}(x+\delta, y')$. Similarly, $\mathcal{G}(x+\delta) = y \iff \ell_{\mathcal{G}}(x+\delta, y) < \min_{y' \in \mathcal{L}: y' \neq y} \ell_{\mathcal{G}}(x+\delta, y')$. Following Taylor's Theorem with Lagrange remainder, we have

$$\ell_{\mathcal{F}}(x+\delta, y) = \ell_{\mathcal{F}}(x,y) + \delta \nabla_x \ell_{\mathcal{F}}(x,y) + \frac{1}{2} \xi^\top \mathbf{H}_{\mathcal{F}} \xi, \tag{6}$$
$$\ell_{\mathcal{G}}(x+\delta, y) = \ell_{\mathcal{G}}(x,y) + \delta \nabla_x \ell_{\mathcal{G}}(x,y) + \frac{1}{2} \xi^\top \mathbf{H}_{\mathcal{G}} \xi. \tag{7}$$

In Eq. (6) and Eq. (7), $\|\xi\| < \|\delta\|$. $\mathbf{H}_{\mathcal{F}}$ and $\mathbf{H}_{\mathcal{G}}$ are Hessian matrices of $\ell_{\mathcal{F}}$ and $\ell_{\mathcal{G}}$ respectively.

Since $\ell_{\mathcal{F}}(x+\delta, y)$ and $\ell_{\mathcal{G}}(x+\delta, y)$ have upper smoothness $\overline{\sigma}_{\mathcal{F}}$ and $\overline{\sigma}_{\mathcal{G}}$, the maximum eigenvalues of $\mathbf{H}_{\mathcal{F}}$ and $\mathbf{H}_{\mathcal{G}}$ (both defined generally) are bounded. As the result, $\left|\xi^\top \mathbf{H}_{\mathcal{F}} \xi\right| \leq \overline{\sigma}_{\mathcal{F}} \cdot \|\xi\|_2^2 \leq \overline{\sigma}_{\mathcal{F}} \epsilon^2$. Applying them to Eq. (6) and Eq. (7), we thus have

$$\ell_{\mathcal{F}} + \delta \nabla_x \ell_{\mathcal{F}} - \frac{\overline{\sigma}_{\mathcal{F}} \epsilon^2}{2} \leq \ell_{\mathcal{F}}(x+\delta, y) \leq \ell_{\mathcal{F}} + \delta \nabla_x \ell_{\mathcal{F}} + \frac{\overline{\sigma}_{\mathcal{F}} \epsilon^2}{2}, \tag{8}$$
$$\ell_{\mathcal{G}} + \delta \nabla_x \ell_{\mathcal{G}} - \frac{\overline{\sigma}_{\mathcal{G}} \epsilon^2}{2} \leq \ell_{\mathcal{G}}(x+\delta, y) \leq \ell_{\mathcal{G}} + \delta \nabla_x \ell_{\mathcal{G}} + \frac{\overline{\sigma}_{\mathcal{G}} \epsilon^2}{2}. \tag{9}$$

Here we abbreviate the notations $\nabla_x \ell_{\mathcal{G}}(x,y)$ and $\nabla_x \ell_{\mathcal{F}}(x,y)$ as $\nabla_x \ell_{\mathcal{G}}$ and $\nabla_x \ell_{\mathcal{F}}$ respectively to save space, as often needed hereinafter. Apply right hand side of Eq. (8)

to $\Pr\left(\mathcal{F}\left(x+\delta\right)=y\right)\leq\alpha$:

$$\begin{aligned}
&\Pr\left(\mathcal{F}\left(x+\delta\right)=y\right)\\
=&\Pr\left(\ell_{\mathcal{F}}\left(x+\delta,y\right)<\min_{y'\in\mathcal{L}:y'\neq y}\ell_{\mathcal{F}}(x+\delta,y')\right)\\
\geq&\Pr\left(\ell_{\mathcal{F}}+\delta\nabla_x\ell_{\mathcal{F}}+\frac{1}{2}\overline{\sigma}_{\mathcal{F}}\epsilon^2<\min_{y'\in\mathcal{L}:y'\neq y}\ell_{\mathcal{F}}(x+\delta,y')\right)\\
=&\Pr\left(\delta\cdot\frac{\nabla_x\ell_{\mathcal{F}}}{\|\nabla_x\ell_{\mathcal{F}}\|_2}<f(x,y)\right),\\
\Longrightarrow&\Pr\left(\delta\cdot\frac{\nabla_x\ell_{\mathcal{F}}}{\|\nabla_x\ell_{\mathcal{F}}\|_2}<f(x,y)\right)\leq\alpha.
\end{aligned}\tag{10}$$

Apply left hand side of Eq. (9) to $\Pr\left(\mathcal{G}\left(x+\delta\right)=y\right)$:

$$\begin{aligned}
&\Pr\left(\mathcal{G}\left(x+\delta\right)=y\right)\\
=&\Pr\left(\ell_{\mathcal{G}}\left(x+\delta,y\right)<\min_{y'\in\mathcal{L}:y'\neq y}\ell_{\mathcal{G}}(x+\delta,y)\right)\\
\leq&\Pr\left(\ell_{\mathcal{G}}+\delta\nabla_x\ell_{\mathcal{G}}-\frac{1}{2}\overline{\sigma}_{\mathcal{G}}\epsilon^2<\min_{y'\in\mathcal{L}:y'\neq y}\ell_{\mathcal{G}}(x+\delta,y)\right)\\
=&\Pr\left(\delta\cdot\frac{\nabla_x\ell_{\mathcal{G}}}{\|\nabla_x\ell_{\mathcal{G}}\|_2}<g(x,y)\right)\\
\leq&\Pr\left(\delta\cdot\frac{\nabla_x\ell_{\mathcal{G}}}{\|\nabla_x\ell_{\mathcal{G}}\|_2}<c_{\mathcal{G}}\right).
\end{aligned}\tag{11}$$

Eq. (11) use the definition of g in Eq. (4) and the definition of $c_{\mathcal{G}}$. Since $\|\delta\|_2\leq\epsilon$, using Lemma 1, we can deduce

$$\delta\cdot\frac{\nabla_x\ell_{\mathcal{G}}}{\|\nabla_x\ell_{\mathcal{G}}\|_2}<f(x,y)-\epsilon\sqrt{2-2\underline{\mathcal{S}}_{\mathcal{D}}\left(\ell_{\mathcal{F}},\ell_{\mathcal{G}}\right)}\tag{12}$$

$$\Longrightarrow\delta\cdot\frac{\nabla_x\ell_{\mathcal{G}}}{\|\nabla_x\ell_{\mathcal{G}}\|_2}<f(x,y)-\epsilon\sqrt{2-2\cos\left\langle\nabla_x\ell_{\mathcal{F}},\nabla_x\ell_{\mathcal{G}}\right\rangle}\tag{13}$$

$$\Longrightarrow\delta\cdot\frac{\nabla_x\ell_{\mathcal{F}}}{\|\nabla_x\ell_{\mathcal{F}}\|_2}<f(x,y).\tag{14}$$

From Eq. (12) to Eq. (13), the definition of $\underline{\mathcal{S}}_{\mathcal{D}}$ is used, since it indicates that $\underline{\mathcal{S}}_{\mathcal{D}}\left(\ell_{\mathcal{F}},\ell_{\mathcal{G}}\right)\leq\cos\left\langle\nabla_x\ell_{\mathcal{F}}\left(x,y\right),\nabla_x\ell_{\mathcal{G}}\left(x,y\right)\right\rangle$. Eq. (13) to Eq. (14) uses the Lemma directly. As a result, using Eq. (10), we have

$$\begin{aligned}
&\Pr\left(\delta\cdot\frac{\nabla_x\ell_{\mathcal{G}}\left(x,y\right)}{\|\nabla_x\ell_{\mathcal{G}}\left(x,y\right)\|_2}<f(x,y)-\epsilon\sqrt{2-2\underline{\mathcal{S}}_{\mathcal{D}}\left(\ell_{\mathcal{F}},\ell_{\mathcal{G}}\right)}\right)\\
\leq&\Pr\left(\delta\cdot\frac{\nabla_x\ell_{\mathcal{F}}\left(x,y\right)}{\|\nabla_x\ell_{\mathcal{F}}\left(x,y\right)\|_2}<f(x,y)\right)\leq\alpha.
\end{aligned}$$

Since $c_{\mathcal{F}}\leq f(x,y)$, we also have

$$\Pr\left(\delta\cdot\frac{\nabla_x\ell_{\mathcal{G}}\left(x,y\right)}{\|\nabla_x\ell_{\mathcal{G}}\left(x,y\right)\|_2}<c_{\mathcal{F}}-\epsilon\sqrt{2-2\underline{\mathcal{S}}_{\mathcal{D}}\left(\ell_{\mathcal{F}},\ell_{\mathcal{G}}\right)}\right)\leq\alpha.$$

Given the minimum of $\delta\cdot\frac{\nabla_x\ell_{\mathcal{G}}(x,y)}{\|\nabla_x\ell_{\mathcal{G}}(x,y)\|_2}$ is lower bounded by $-\max\|\delta\|_2=-\epsilon$. Therefore, its expectation can be bounded:

$$\mathbb{E}\left[\delta\cdot\frac{\nabla_x\ell_{\mathcal{G}}}{\|\nabla_x\ell_{\mathcal{G}}\|_2}\right]\geq-\epsilon\alpha+\left(c_{\mathcal{F}}-\epsilon\sqrt{2-2\underline{\mathcal{S}}_{\mathcal{D}}\left(\ell_{\mathcal{F}},\ell_{\mathcal{G}}\right)}\right)(1-\alpha).\tag{15}$$

According to Markov's inequality, from Eq. (15), we can deduce that

$$\begin{aligned}
&\Pr\left(\delta\cdot\frac{\nabla_x\ell_{\mathcal{G}}}{\|\nabla_x\ell_{\mathcal{G}}\|_2}<c_{\mathcal{G}}\right)\\
\leq&\frac{\epsilon(1+\alpha)-\left(c_{\mathcal{F}}-\epsilon\sqrt{2-2\underline{\mathcal{S}}_{\mathcal{D}}\left(\ell_{\mathcal{F}},\ell_{\mathcal{G}}\right)}\right)(1-\alpha)}{\epsilon-c_{\mathcal{G}}}.
\end{aligned}\tag{16}$$

Combining Eq. (11) and Eq. (16), we have

$$\begin{aligned}
&\Pr\left(\mathcal{G}\left(x+\delta\right)=y\right)\\
\leq&\frac{\epsilon(1+\alpha)-\left(c_{\mathcal{F}}-\epsilon\sqrt{2-2\underline{\mathcal{S}}_{\mathcal{D}}\left(\ell_{\mathcal{F}},\ell_{\mathcal{G}}\right)}\right)(1-\alpha)}{\epsilon-c_{\mathcal{G}}}.
\end{aligned}\tag{17}$$

Thus, we conclude our proof by plugging Eq. (17) into Eq. (5). □

A.3. Proof of Connection between *JR* and *IR*

Proposition 1. *Let a neural network parameterized by θ, and f_θ represents its logit network. Given a sample (x,y), if $\|\nabla_x f_\theta(x)\|_F\to 0$, $\|\nabla_x\ell(f_\theta(x),y)\|\to 0$, where ℓ denotes the cross-entropy loss function.*

Proof. Define the logit output of f_θ given input feature x with respect to each class as $z_1,z_2,...,z_k$, including the according logit of target class z_y. Accordingly, $\nabla_x f_\theta(x)=(z_1,z_2,...,z_k)^T$. Thus, we have

$$\|\nabla_x f_\theta(x)\|_F=\sum_i^k\|\nabla_x z_i\|.\tag{18}$$

The cross-entropy loss of (x,y) is computed as follows:

$$\ell(f_\theta(x),y)=-\log(\frac{e^{z_y}}{\sum_i^k e^{z_i}})=-z_y+\log(\sum_i^k e^{z_i}).$$

As a result, the gradient *w.r.t.* x $\nabla_x\ell(f_\theta(x),y)$ is

$$\nabla_x\ell(f_\theta(x),y)=-\nabla_x z_y+\frac{\sum_i^k e^{z_i}\nabla_x z_i}{\sum_i^k e^{z_i}}.$$

Thus,

$$\begin{aligned}
\|\nabla_x\ell(f_\theta(x),y)\|&=\|\frac{1}{\sum_i^k e^{z_i}}\cdot\sum_i^k e^{z_i}\nabla_x z_i-\nabla_x z_y\|\\
&\leq\frac{1}{\sum_i^k e^{z_i}}\cdot\|\sum_i^k e^{z_i}\nabla_x z_i\|+\|\nabla_x z_y\|\\
&\leq\frac{1}{\sum_i^k e^{z_i}}\cdot\sum_i^k e^{z_i}\|\nabla_x z_i\|+\|\nabla_x z_y\|\\
&<\sum_i^k\|\nabla_x z_i\|+\|\nabla_x z_y\|.
\end{aligned}\tag{19}$$

Note that if $\sum_i^k\|\nabla_x z_i\|\to 0,\|\nabla_x z_y\|\to 0$. Observing Eqs. (18) and (19), we can conclude that if $\|\nabla_x f_\theta(x)\|_F\to 0$, $\|\nabla_x\ell(f_\theta(x),y)\|\to 0$. □

Appendix B.
Meta-Review

B.1. Summary

The paper investigates the reasons for adversarial transferability from the surrogate model's point of view—that is, how well adversarial examples against a surrogate model (derived from a target model) work against the target model itself. Surrogate models should be smooth, and gradients should be as similar to the original model as possible. However, adversarial transferability is subject to a trade-off between both, as data augmentation for smoothing a model causes data distribution shifts, negatively influencing gradient similarity.

B.2. Scientific Contributions

- Provides a Valuable Step Forward in an Established Field

B.3. Reasons for Acceptance

1) **Comprehensive overview of adversarial transferability.** The paper provides a good overview of different aspects of adversarial transferability, making connections to recent studies in the field. Transferability influences defenses against evasion and thus is essential in recent research. The authors manage to point out the conflicting aspects well.
2) **Relation of gradient similarity (GS) and model smoothness (MS).** The drawn connection of gradient similarity to model smoothness and positioning, both as contradicting properties that require a trade-off, is interesting. Empirically claims are supported well.

B.4. Noteworthy Concerns

1) **Trade-off Conjectures.** The trade-off of gradient similarity (GS) and model smoothness (MS) under adversarial training is based on conjectures.
2) **Comparability of augmentation pro-babilities and Cutout values.** The paper only provides intuition-driven reasoning for why the used augmentation probabilities and the M values of Cutout are comparable.